

AMPED: Adaptive Multi-objective Projection for balancing Exploration and skill Diversification

Geonwoo Cho^{1,*} Jaemoon Lee^{2,*} Jaegyun Im¹ Subi Lee¹ Jihwan Lee¹ Sundong Kim¹
 {gwcho.public, dlwoans0001, soobi1234, jaegyun.public, qhddl2650, sdkim0211}@gmail.com

¹Gwangju Institute of Science and Technology

²Seoul National University

Abstract

Skill-based reinforcement learning (SBRL) enables rapid adaptation in environments with sparse rewards by pretraining a skill-conditioned policy. Effective skill learning requires jointly maximizing both exploration and skill diversity. However, existing methods often face challenges in simultaneously optimizing for these two conflicting objectives. In this work, we propose a new method, Adaptive Multi-objective Projection for balancing Exploration and skill Diversification (AMPED), which explicitly addresses both exploration and skill diversification. We begin by conducting extensive ablation studies to identify and define a set of objectives that effectively capture the aspects of exploration and skill diversity, respectively. During the skill pretraining phase, AMPED introduces a gradient surgery technique to balance the objectives of exploration and skill diversity, mitigating conflicts and reducing reliance on heuristic tuning. In the subsequent fine-tuning phase, AMPED incorporates a skill selector module that dynamically selects suitable skills for downstream tasks, based on task-specific performance signals. Our approach achieves performance that surpasses SBRL baselines across various benchmarks. These results highlight the importance of explicitly harmonizing exploration and diversity and demonstrate the effectiveness of AMPED in enabling robust and generalizable skill learning. <https://geonwoo.me/amped/>

1 Introduction

Efficient exploration remains a major challenge in reinforcement learning (RL), particularly in environments with sparse or delayed rewards [42, 44, 50, 27]. While biological agents naturally discover rewarding behaviors, artificial agents often rely on handcrafted reward functions, which demand extensive domain knowledge and limit scalability [20]. Skill-Based Reinforcement Learning (SBRL) addresses this by pretraining a skill-conditioned policy through unsupervised skill discovery [15, 47], enabling efficient adaptation to downstream tasks.

A common approach in SBRL is to use Unsupervised Reinforcement Learning (URL) objectives during pretraining to discover diverse and useful skills [12, 15]. Two widely used URL methods are: (1) promoting skill diversity by maximizing mutual information (MI) between skills and their state trajectories, and (2) encouraging exploration by maximizing state entropy [24, 30]. (see Appendix A for details.) However, MI-driven objectives often induce premature specialization by curtailing exploration [10, 19, 48], while entropy-based exploration sacrifices skill distinguishability, limiting downstream utility. The core problem is how to balance these competing objectives, ensuring skills remain both distinguishable and broadly exploratory, without resorting to ad-hoc heuristics.

In this work, we bridge two URL paradigms in the theoretical framework of multi-objective reinforcement learning, proposing Adaptive Multi-objective Projection for balancing Exploration and skill

*Equal contribution.

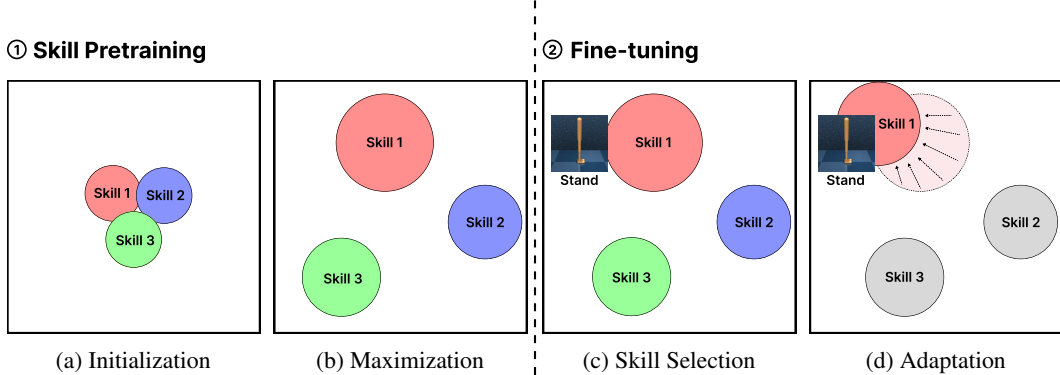


Figure 1: Graphical scheme explaining our method, AMPED. (a) At initialization, the skills exhibit small coverage that are close to each other in the task space. (b) During skill pretraining, exploration and diversity objectives encourage skills to widen and repel each regions. (c) In fine-tuning, the skill selector identifies the skill best aligned with the target task at each step. (d) The selected skill is further adapted via extrinsic rewards to maximize performance on the target task.

Diversification (AMPED). Few previous studies, such as CeSD [5] and ComSD [32], have explored similar integrations but either lack a solid theoretical foundation or exhibit significant limitations (refer to Appendix B).

Our key insight is that gradient conflicts naturally arise between MI-based diversity objectives and entropy-based exploration objectives, leading to inefficient updates that hinder learning [55]. To address this issue, we adopt a gradient surgery method inspired by multi-objective RL, ensuring that conflicting gradient components are removed before applying updates [55]. For each objective, we use particle-based entropy and Random Network Distillation (RND) [8] to drive exploration, and adopt the AnInfoNCE objective for skill diversity. Furthermore, rather than selecting skills uniformly at random during fine-tuning—as is common in prior SBRL approaches [5, 12, 52]—we introduce a Soft Actor-Critic (SAC) based skill selector that learns to select the best matching pretrained skill [17]; and selected skills are also adapted to the task. This adaptive selection manner maximally leverages the inherent diversity of the skill repertoire. A graphical summary of these contributions is provided in Figure 1.

We evaluated AMPED across a range of environments, including toy benchmarks and the Unsupervised Reinforcement Learning Benchmark (URLB) [25]. Specifically, in URLB, AMPED improves the interquartile-mean (IQM) performance over the next-best baselines by: 17.96% relative to the skill-differentiation method BeCL; 15.02% and 9.73% relative to the entropy-maximization methods CIC and APT, respectively; 20.91% and 35.01% relative to the hybrid methods CeSD and ComSD. These results demonstrate that explicitly resolving exploration–diversity gradient conflicts yields substantial gains in SBRL. Ablation studies further confirm that each component of our framework—entropy bonuses, RND, Augmented InfoNCE, gradient surgery, and the skill selector—contributes meaningfully to overall performance. Ultimately, the gradient surgery used to balance exploration and skill diversity can be applied to any other objectives or fields with minimal architectural changes.

We provide the full implementation of AMPED to facilitate the reproduction of our main results at <https://github.com/Cho-Geonwoo/amped>.

2 Preliminaries

2.1 Markov decision process (MDP) and Conditional MDP (CMDP)

MDP is a tuple $\mathcal{M} := (\mathcal{S}, \mathcal{A}, P, R, \mu, \gamma)$, where \mathcal{S} is a state space; \mathcal{A} is an action space; $P : \mathcal{S} \times \mathcal{A} \rightarrow \Delta(\mathcal{S})$ is a transition model where we denote the probability of transitioning from s to s' with action a by $P(s'|a, s)$; $R : \mathcal{S} \times \mathcal{A} \rightarrow \mathbb{R}$ is a reward function; $\mu \in \Delta(\mathcal{S})$ is the initial state distribution; and $\gamma \in \mathbb{R}$ is a discount factor. A trajectory is a sequence of states and actions, for example: $\tau = (s_1, a_1, s_2, a_2, \dots, a_{H-1}, s_H)$. We will only consider finite horizon MDP, i.e. $H < \infty$. A policy $\pi : \mathcal{S} \rightarrow \Delta(\mathcal{A})$ maps states to action probabilities, denoted as $\pi(a|s)$.

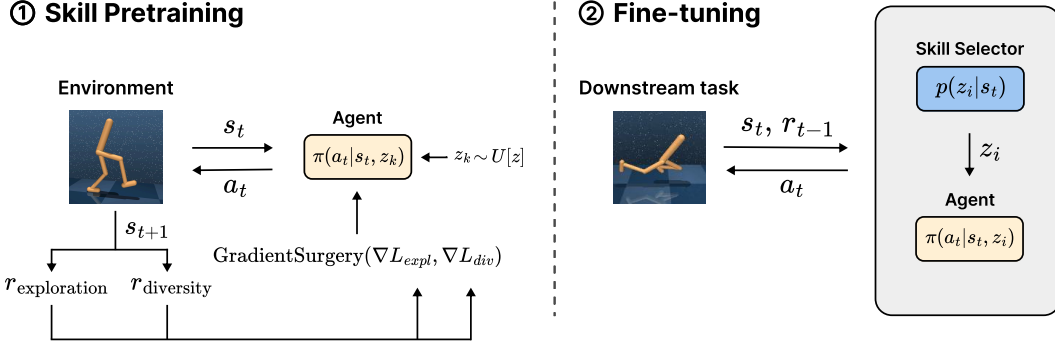


Figure 2: Overview of the training process of AMPED. During the skill pretraining phase, the agent is conditioned on randomly sampled skills and optimized using intrinsic rewards for exploration and diversity. These gradients not directly used, but are balanced via a gradient surgery mechanism. In fine-tuning phase, a skill selector adaptively selects skills on each step, based on task-specific feedback, and the agent is further optimized using extrinsic rewards from the downstream target task.

CMDP extends MDP by introducing a latent variable $z \in \mathcal{Z}$, often representing a skill or context. The policy becomes $\pi(a|s, z)$, additionally conditioned on z . CMDP is used in skill discovery, where the goal is to learn diverse, distinct behaviors parameterized by z .

Both MDP and CMDP aim to maximize the expected cumulative discounted reward: $\max_{\pi} \mathbb{E}_{\tau \sim (\pi, P)} [\sum_t \gamma(t) r_t]$ where trajectory τ is generated from policy π .

2.2 Entropy and Mutual Information

For random variables X, Y , Shannon entropy and MI are defined as $H(X)$, $I(X; Y)$, respectively:

$$H(X) = -E[\log p(X)], \quad I(X; Y) = D_{\text{KL}}(p_{X,Y} \parallel p_X p_Y) \quad (1)$$

where D_{KL} is a Kullback–Leibler divergence, and $p_{X,Y}$ is a joint distribution. Higher entropy corresponds to higher unpredictability, the state distribution becomes more uniform in the state space, thereby facilitating broader exploration. In contrast, higher MI indicates stronger statistical dependence between two random variables. MI is commonly used between skills and trajectories, so that each skills reliably produces its characteristic behavior. Moreover, by using contrastive learning to estimate MI, each skills repel the others, thereby achieving skill diversity.

These information-theoretic terms are widely used as an intrinsic objective in URL. For example, CIC [24]: $I(\tau; z)$, DIAYN [12]: $I(S; Z) + H(A|S) - I(A; Z|S)$, BeCL [52]: $I(S^{(1)}; S^{(2)})$; see Appendix C for additional details.

2.3 Gradient Conflict

In multi-objective RL, optimizing multiple objectives simultaneously with the same network can lead to conflicts between the gradients of each objective. A naive implementation computes the gradients for each objective independently and performs gradient descent using their sum. However, this can result in gradient conflict, where the update direction that benefits one task negatively impacts another [55].

To address this issue, Yu et al. [55] proposed PCGrad, a gradient surgery method designed to mitigate such conflicts by removing interfering gradient components. Given a set of objectives $\mathcal{L}_k(\theta)$ for $k = 1, \dots, n$, the corresponding gradients are first computed as $g_k = \nabla_{\theta} \mathcal{L}_k$. The gradients are then processed sequentially in a random order. For each pair of gradients g_i and g_k , if a conflict is detected—i.e., if $g_i \cdot g_k < 0$ —then the projection of g_i onto g_k is subtracted from g_i . Thus, the modified gradient is guaranteed not to interfere with the descent directions of other tasks. Moreover, PCGrad paper showed that under appropriate conditions, a projected gradient step can outperform standard stochastic gradient descent (SGD). Finally, the adjusted gradients are aggregated and applied using conventional SGD.

3 Adaptive Multi-objective Projection for Exploration and Diversification (AMPED)

Our goal is to maximize both skill diversity and exploration, as supported by prior works [12, 15, 52, 53]. Previous methods in URL, such as CeSD and ComSD [5, 32], have combined these objectives. Following this approach, we optimize the discounted cumulative return $\mathbb{E}[\sum_t \gamma^t (r_{\text{exploration}} + r_{\text{diversity}})]$, using a DDPG agent [26]. Here, $r_{\text{exploration}}$ incorporates entropy and RND-based objectives [8], while $r_{\text{diversity}}$ includes the AnInfoNCE term [43]. The specific formulations and the rationale for their use are detailed in Section 3.2. We illustrate our overall method in Figure 2.

Maximizing state entropy is essential because it induces a uniform visitation distribution, minimizing worst-case regret as shown by Gupta et al. [16]. And this principle has been empirically validated in prior works [18, 30]. We now briefly motivate the importance of skill diversity for downstream tasks via the following theoretical analysis.

3.1 Theoretical Analysis of Skill Diversity

Assume a finite state space \mathcal{S} with cardinality S , and a finite horizon H . Suppose we are given skill-conditioned policies $\pi(a | s, z)$ with a finite number of skills and a downstream task. Let π^* be the optimal policy and $\rho^* \in \Delta(\mathcal{S}^H)$ be a corresponding state distribution. Also set z_* as a best policy in the sense that $z_* = \operatorname{argmin}_z d(\rho^*, \rho_z)$. We denote the total variation of two probability distributions by $d(\rho_1, \rho_2) = \frac{1}{2} \|\rho_1 - \rho_2\|_1$.

Theorem 1. Define $\delta = \min_{i \neq j} d(\rho_{z_i}, \rho_{z_j})$, $\varepsilon = d(\rho^*, \rho_{z_*})$. Assume that the skills are sufficiently diversified, so that $\Delta \equiv \delta - 2\varepsilon > 0$.

Draw n i.i.d. roll-outs from optimal policy $S^{(1)}, \dots, S^{(n)} \sim \rho^*$ and form the empirical distribution $\hat{\rho}$. Consider the greedy skill selector $\hat{z} := \operatorname{argmin}_z d(\hat{\rho}, \rho_z)$. Then

$$\Pr[\hat{z} \neq z_*] \leq 2^{S^H} \exp\left(-\frac{n\Delta^2}{2}\right) \quad (2)$$

In terms of confidence level $\eta \in (0, 1)$, if

$$n \geq \frac{2}{\Delta^2} (S^H \log 2 - \log \eta) \quad (3)$$

we have $\Pr[\hat{z} \neq z_*] \leq \eta$.

Thus, higher diversity δ improves the margin Δ and drives the required sample count down. This formalizes the intuition that diverse skills make it statistically easier to identify the skill which, when conditioned upon, yields a policy closest to the downstream optimal policy π^* . This theorem is proved in the Appendix D.

3.2 Exploration & Diversity Intrinsic Rewards

Exploration Reward The exploration reward consists of two key components: an entropy-based term and a RND term [8]. The entropy component, widely used in SBRL [15, 24, 29], enhances exploration when maximized and is defined as $H(S_{\text{tot}})$, where the discounted total state distribution is given by $S_{\text{tot}}(s) = (1 - \gamma) \sum_t \gamma^t p(s_t = s)$. Since the exact entropy computation is intractable due to the unknown discounted total state distribution, we approximate it using a particle-based method from [24]. Each particle is an embedded state pair $x_i = g_{\psi_1}(\tau_i)$ where $\tau_i = (s_t, s_{t+1})$ and g_{ψ_1} denotes the embedding function. Then the density is estimated by distances to its k th nearest neighbor, $R_{i,k,n}$. The intrinsic reward is then computed as $r_{\text{entropy}}(s) = \log\left(\sum_{l=1}^k R_{i,l,n}\right)$, which captures the entropy contribution of each particle in the state space.

To construct a meaningful latent space, we train an encoder with the contrastive loss:

$$\mathcal{L}_{\text{CIC}}(\tau) = \frac{g_{\psi_1}(\tau_i)^\top g_{\psi_2}(z_i)}{\|g_{\psi_1}(\tau_i)\| \|g_{\psi_2}(z_i)\| T} - \log \frac{1}{N} \sum_{j=1}^N \exp\left(\frac{g_{\psi_1}(\tau_j)^\top g_{\psi_2}(z_i)}{\|g_{\psi_1}(\tau_j)\| \|g_{\psi_2}(z_i)\| T}\right), \quad (4)$$

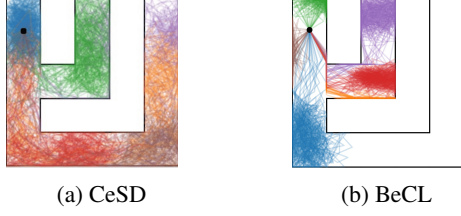


Figure 3: Exploration trajectories in the square maze with six skills. CeSD yields more contiguous coverage, while BeCL enforces stronger separation, leaving noticeable gaps.

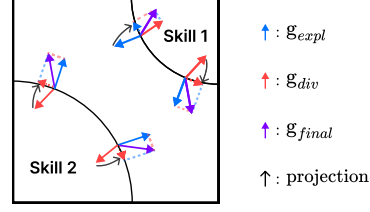


Figure 4: Graphical illustration of gradient surgery. When diversity gradient (red) and exploration gradient (blue) conflict, one gradient is randomly projected onto the orthogonal complement of the other to balance updates. Added gradient (purple) is used for update of parameters.

here g_{ψ_2} encodes skills, and $T > 0$ is a temperature hyperparameter, adapted from CIC [24].

Despite its benefits, entropy-based exploration alone is insufficient in high-dimensional spaces due to its $\mathcal{O}(n^2)$ complexity, making full-state utilization impractical. Although clipping the particle number alleviates computational overhead, it correspondingly degrades the fidelity of the entropy approximation. To address this, we integrate RND, a model-based exploration technique, which is effective in later training stages when sufficient data is available for model learning. RND trains a predictor network f_θ to approximate the output of a fixed, randomly initialized target network f_{target} , with the intrinsic reward $r_{\text{rnd}}(s) = \|f_\theta(s) - f_{\text{target}}(s)\|^2$, where higher prediction error indicates unfamiliar states, encouraging exploration.

We define the exploration reward as a linear combination of the RND and entropy terms. Specifically, $r_{\text{exploration}}(s) = \alpha r_{\text{entropy}}(s) + \beta r_{\text{rnd}}(s)$ where α and β is the positive scaling coefficients that modulate the relative influence of the entropy-based and RND rewards. Ablation studies in Section 4.3 confirm that combining entropy and RND significantly improves exploration efficiency in high-dimensional environments.

Diversity Reward To motivate our diversity reward formulation, we first examine CeSD [5]. CeSD optimizes $H(S_{\text{tot}}) + \mathcal{L}_{\text{diversity}}$, where $\mathcal{L}_{\text{diversity}}$ ensures non-overlapping skill trajectories. However, if the supports of different skill coverages become disjoint, the diversity loss $\mathcal{L}_{\text{diversity}}$ no longer enforces inter-skill distributional separation, which can lead to skill clustering rather than promoting broad coverage of the state space.

To overcome this limitation, we adopt the MI objective $I(S^{(1)}, S^{(2)})$ from BeCL [52], where $S^{(1)}$ and $S^{(2)}$ are states sampled from trajectories generated by the same skill. Unlike CeSD’s heuristic penalty, this formulation actively repels skill distributions, leading to stronger skill separation. Moreover, they showed that sufficiently maximizing the BeCL objective also increases state entropy, balancing exploration and diversity. The empirical results of the 2D maze experiment (As shown in Figure 3) confirm its superiority in differentiating skills compared to CeSD. For an analysis of the effectiveness of skill diversification under BeCL’s MI objective, refer to Appendix E.

For MI estimation, we use AnInfoNCE [43], an anisotropic variant of InfoNCE [35], designed to handle asymmetries in latent factors. Empirical studies (Section 4.3) demonstrate its advantage over standard InfoNCE.

The AnInfoNCE loss is defined as:

$$\mathcal{L}_{\text{AINCE}}(f, \hat{\Lambda}) = -\mathbb{E}_{s, s^+, \{s_i^-\}} \left[\ln \frac{e^{-\|f(s^+) - f(s)\|_{\hat{\Lambda}}^2}}{e^{-\|f(s^+) - f(s)\|_{\hat{\Lambda}}^2} + \sum_{i=1}^M e^{-\|f(s_i^-) - f(s)\|_{\hat{\Lambda}}^2}} \right], \quad (5)$$

where s, s^+ are positive samples (from the same skill), and $\{s_i^-\}$ are negative samples (from different skills). The matrix $\hat{\Lambda}$ is a learnable diagonal matrix, and the augmented norm is defined as $\|x\|_{\hat{\Lambda}}^2 = x^T \hat{\Lambda} x$. The state encoder f and $\hat{\Lambda}$ are updated via loss minimization. Accordingly, we define contrastive reward $r_{\text{diversity}}$ as the term inside the bracket.

3.3 Balancing Exploration and Diversity Objectives

Differentiable skills improve adaptability in dynamic skill selection but often compromise exploration ability [52], leading to suboptimal performance in environments. By treating MI, entropy, and RND as distinct objectives, our problem can be framed as a multi-objective RL setting, in which all three objectives are optimized concurrently. In this perspective, observed gradient interference can be interpreted as a form of *gradient conflict*, a well-documented challenge in multi-objective RL. Empirical evidence of such conflicts in our setting is presented in Table 1.

Table 1: Gradient conflict ratio in skill learning across environments. The ratio is defined as the fraction of training steps exhibiting gradient conflicts, averaged over 10 random seeds for the Walker, Quadraped, and Jaco tasks reported as mean \pm standard deviation.. One can observe that conflicts arise with high probability.

	Walker	Quadraped	Jaco
Gradient Conflict Ratio	0.754 ± 0.281	0.907 ± 0.103	0.958 ± 0.056

To mitigate this issue, we integrate a gradient projection method, known as gradient surgery or projecting conflicting gradients (PCGrad), proposed by Yu et al. [55]. The key idea (Visualized in Figure 4) is to remove gradient interference by projecting one objective’s gradient onto the orthogonal complement of the other. Concretely, let g_{expl} and g_{div} denote exploration and diversity gradient, respectively. At each update, we first randomly choose which gradient to adjust: with probability p we project g_{expl} to g_{div} , and with probability $1 - p$ vice versa. Then, the final update gradient g_{final} is obtained by summing two gradients, one projected. The procedure is detailed in Algorithm 1. Although more advanced methods exist (e.g., Liu et al. [28], Navon et al. [33]), we opted for the original gradient surgery approach due to its simplicity and ease of integration. Despite its straightforward design, this method proved sufficiently effective in mitigating gradient conflicts for our application.

3.4 Adaptive Skill Selection

To utilize the diversity of skill set, we adopt a skill selection method during fine-tuning. Specifically, we train a skill selector $p(z|s)$ concurrently with skill fine-tuning. At every time step, the selector samples a skill according to $p(z|s)$, while the policy conditioned on that selected skill continues to adapt under the downstream task reward. We employ an ϵ -greedy strategy with ϵ decaying over the course of training to balance between exploring new skills and exploiting high-performing ones.

Prior methods often impose constraints to stabilize skill learning. For example, DIAYN [12] freezes the prior distribution, VIC [15] fixes the skill at initialization, and other approaches rely on labeled demonstrations. In contrast, our method jointly trains the policy and skill distribution, which turned out to be stable and effective.

During evaluation, the skill selector becomes deterministic, employing a greedy strategy to maximize task performance. This hierarchical framework facilitates efficient skill transfer and adaptation while maintaining decision stability. Detailed descriptions of the implementation of the skill selector are provided in Appendix F.4.

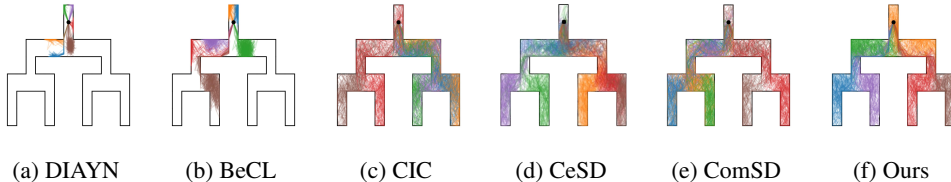


Figure 5: Agents exploring on Tree Maze after pretrained from different skill discovery objectives. From (a) to (f) each are trained with 6 skills, and the method used to train is: (a) DIAYN, (b) BeCL, (c) CIC, (d) CeSD, (e) ComSD, (f) AMPED (Ours). Visually, our approach exhibits the most distinct skills while ensuring full coverage of the state space.

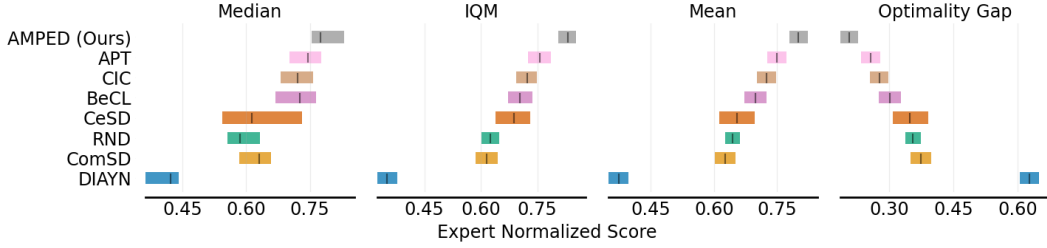


Figure 6: Aggregated expert-normalized performance on 12 URLB downstream tasks after 100k finetuning steps, averaged over 10 random seeds. Four metrics—median, IQM, arithmetic mean, and optimality gap—are plotted using the evaluation protocol introduced by Agarwal et al. [1]. Our method (gray) achieves the highest median, IQM, and mean scores and the smallest optimality gap, outperforming the previous state-of-the-art APT (pink) and other baselines.

4 Experiments

In this section, we provide a comprehensive evaluation of our method’s performance in comparison with baseline approaches using the URLB. We also illustrate skill visualizations in the Tree Maze, which reveal how our method explores and separates behaviors. A series of targeted ablations then isolates the impact of each algorithmic component—RND, AnInfoNCE, gradient surgery, and skill selector. We conclude by visualizing representative skills learned during URLB pretraining.

4.1 Skill Discovery in Tree Maze

The experiment demonstrating the skill discovery capability is conducted in a Tree Maze environment [10]. For details on the environment, implementations, and hyperparameters, refer to the Appendix F. The Tree Maze serves as a toy environment for preliminary analysis and insight; accordingly, we evaluate a reduced set of baselines, DIAYN, BeCL, CIC, CeSD, and ComSD, compared to those used in URLB. Refer to the Appendix C for comprehensive details on the baselines.

Figure 5 illustrates the visualization of each baseline’s performance after pretraining with six skills. In terms of skill distinguishability, our observations indicate that DIAYN, BeCL are capable of learning distinct skills, enabling clear differentiation among the states covered by each skill. Conversely, the skills learned by CIC are less distinguishable, likely due to the absence of a skill-differentiating term in its reward function. Regarding state coverage, CIC, CeSD and ComSD nearly reach the state coverage limit, whereas DIAYN and BeCL exhibit inferior performance in this regard. Notably, our proposed method, AMPED, demonstrates superior performance in both maximizing skill discriminability and state coverage, achieving the state coverage limit while each skill clearly separated. Additional experiments on the effect of varying the number of skills, results in other maze layout, and the evolution of skills over training steps are provided in Appendix G.

4.2 Evaluation on URLB

To evaluate the performance of our method on downstream tasks, we utilize 12 tasks from the URLB. The benchmark comprises three domains: Walker, Quadruped, and Jaco. Detailed descriptions of the URLB are provided in Appendix F.3. Each method is first pretrained for 200K steps using an intrinsic reward, followed by fine-tuning for 100K steps on the downstream tasks.

For comparative evaluation, we selected strong baseline methods from the URLB, including DIAYN, APT, BeCL, CIC, RND, and the recently proposed CeSD and ComSD. Furthermore, methods such as LSD [36], CSD [37], and Metra [38] were omitted because they do not exhibit performance improvements on the URLB relative to CeSD [5]. Our implementation adheres to the official URLB code [23]. Additional information on hyperparameters and network architectures can be found in Appendix F. For more details on reproducing these baselines, see Appendix F.8.

In order to ensure a fair comparison, we fine-tuned all methods under identical conditions without using the skill selector. Each method was pretrained with 10 random seeds, resulting in a total of 1080 runs (10 seeds \times 9 methods \times 12 tasks). The aggregation of statistics was performed using the

Reliable open-source framework [1]. The expert score, which is used to calculate these metrics, was derived from an expert DDPG agent, as outlined in [1].

As shown in Figure 6, our method achieves the best results on the URLB. As recommended by Agarwal et al. [1], we use the IQM as our primary performance measure. In particular, it surpasses the skill-differentiating methods BeCL by 17.96%, the entropy-maximization method CIC and APT by 15.02%, 9.73%, respectively, as well as the recent diversity–exploration hybrids CeSD and ComSD by 20.91%, 35.01%, respectively. These results suggest that considering both diversity and exploration is critical for downstream task performance, and more importantly, appropriately balancing these objectives is essential. All scores of each method at each task is reported at the Appendix H.

Table 2: Episode returns under component ablation (averaged over 10 seeds) across the Walker, Quadruped, and Jaco benchmarks. Ablating any single component—RND, AnInfoNCE loss, gradient surgery, or the skill selector—occasionally improves performance on individual tasks, yet yields degraded overall returns. The best result is shown in **bold**, and the second-best is underlined.

Domain	Task	AMPED (Ours)	w.o. RND	w.o. AnInfoNCE	w.o. Gradient Surgery	w.o. Skill Selector
Walker	Flip	674 ± 105	487 ± 47	536 ± 75	625 ± 48	686 ± 133
	Run	467 ± 103	341 ± 67	440 ± 41	427 ± 57	517 ± 49
	Stand	951 ± 38	917 ± 67	<u>950 ± 25</u>	939 ± 26	947 ± 19
	Walk	929 ± 19	638 ± 60	<u>923 ± 18</u>	899 ± 45	886 ± 63
	Sum	<u>3021</u>	2383	2849	2890	3036
Quadruped	Jump	720 ± 32	597 ± 154	<u>705 ± 22</u>	641 ± 64	699 ± 68
	Run	494 ± 53	410 ± 84	496 ± 37	453 ± 13	493 ± 54
	Stand	906 ± 67	<u>905 ± 10</u>	867 ± 70	890 ± 34	816 ± 150
	Walk	890 ± 59	611 ± 228	<u>870 ± 26</u>	747 ± 114	816 ± 116
	Sum	3010	2523	<u>2938</u>	2731	2824
Jaco	Re. bottom left	<u>143 ± 32</u>	147 ± 14	105 ± 33	111 ± 27	139 ± 34
	Re. bottom right	144 ± 25	132 ± 40	148 ± 14	114 ± 35	140 ± 21
	Re. top left	<u>140 ± 39</u>	163 ± 36	<u>140 ± 23</u>	96 ± 23	130 ± 38
	Re. top right	154 ± 46	144 ± 47	92 ± 24	106 ± 49	<u>146 ± 49</u>
	Sum	<u>581</u>	586	485	427	555

4.3 Component-Wise Ablation Analysis

Each component’s impact is quantified by individually ablating it within AMPED and reporting the resulting relative change in total returns (see Table 2). In the Walker domain, removing RND incurs a 21.1% drop; in Quadruped it costs 16.2%; in Jaco, 0.9% increased but it is negligible, confirming RND’s crucial exploration role. Dropping the AnInfoNCE diversity term reduces Walker by 5.7%, Quadruped by 2.4%, and Jaco by 16.5%, underscoring the need for skill separation. Disabling gradient surgery degrades returns by 4.3% (Walker), 9.3% (Quadruped), and 26.5% (Jaco), highlighting the value of conflict resolution. Finally, omitting the skill selector yields a 0.5% gain in Walker but decreases Quadruped by 6.2% and Jaco by 4.5%, demonstrating the importance of the skill selector.

Collectively, these ablations confirm that each component—RND, contrastive diversity, gradient surgery, and skill selection—makes a non-redundant and substantial contribution to the overall efficacy of AMPED.

4.4 Effect of Projection Ratio on Gradient Conflict Resolution

In Figure 7, we compare three projection strategies: always projecting the exploration gradient onto the diversity gradient ($p = 0.0$), always projecting the diversity gradient onto the exploration gradient ($p = 1.0$), and our AMPED approach with projection ratio described in Appendix F.5. AMPED achieves the highest aggregate returns in all three domains; the extreme strategies sometimes excel on individual tasks but suffer sharp drops elsewhere, lowering overall returns. These results confirm that a balanced projection ratio effectively mitigates gradient conflicts and consistently improves

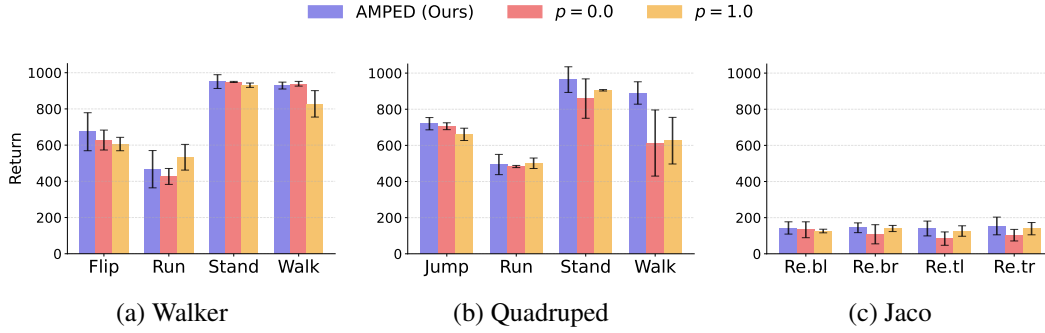


Figure 7: Task-level return comparison under different projection ratios. This figure shows ablation results across individual tasks in the Walker, Quadruped, and Jaco domains, comparing AMPED with fixed projection settings ($p = 0.0$, $p = 1.0$). Each bar indicates the mean, and error bars represent the standard deviation. AMPED results are computed over 10 random seeds, while the $p = 0.0$ and $p = 1.0$ variants use 3 seeds each. In the Jaco domain, task labels “Re.bl”, “Re.br”, “Re.tl”, and “Re.tr” refer to reaching the bottom-left, bottom-right, top-left, and top-right targets, respectively.

skill-learning across diverse environments. Detailed result can be found at Appendix H. For further ablation on the effects of reward-scaling factors in URLB, refer to Appendix I.

4.5 Visualization of Skills

We visualized the skills learned by our method during the pretraining phase on the URLB. A variety of meaningful skills—such as getting up from the ground, stepping forward, backward somersault—were identified. Figure 8 illustrates one of the non-trivial skills; a broader collection of skills is available in the Appendix L. The ability to acquire diverse skills that are potentially useful for downstream tasks contributes to the superior performance observed in many downstream tasks, as shown in Figure 6.



Figure 8: Forward somersault behavior acquired during the skill pretraining stage.

5 Conclusion

In this work, we introduce AMPED to address the dual objectives of exploration and skill diversity in SBRL. Our framework unifies entropy-based exploration with contrastive skill separation, explicitly resolves their gradient conflicts via PCGrad for more stable updates, and employs a skill selector to adaptively deploy skills during fine-tuning. Empirically, we show that (i) eliminating exploration–diversity gradient interference is crucial, (ii) combining AnInfoNCE-inspired diversity losses with RND-driven entropy bonuses yields a robust balance between competing incentives, and (iii) our skill selector meaningfully boosts downstream performance. Complementing these findings, we also presented a theoretical analysis highlighting the critical role of skill diversity in optimizing downstream returns.

While AMPED was developed for skill-based RL, its core insight, treating exploration and diversity as competing objectives and resolving their gradient conflicts via projection, offers a powerful lens for any domain confronting multiple learning signals. By demonstrating its efficacy in SBRL, we hope to inspire broader adoption of gradient-projection methods across machine learning and beyond.

Future research could adopt more advanced conflict-resolution techniques and remove remaining heuristics, develop more precise estimators for our objectives, or identify alternative objective functions that better reconcile exploration and diversity. Additionally, investigators might explore factors beyond exploration and diversity or address the fixed-skill-count limitation of our current framework. Further details are available in Appendix M. By tackling these challenges, the SBRL community can progress toward creating richer, more capable agents.

References

- [1] Rishabh Agarwal, Max Schwarzer, Pablo Samuel Castro, Aaron C Courville, and Marc Bellemare. Deep reinforcement learning at the edge of the statistical precipice. *Advances in Neural Information Processing Systems*, 34:29304–29320, 2021.
- [2] Ziqiao Ao and Jinglai Li. Entropy estimation via normalizing flow. In *Proceedings of the AAAI Conference on Artificial Intelligence*, volume 36, pages 9990–9998, 2022.
- [3] Akhil Bagaria, Jason K Senthil, and George Konidaris. Skill discovery for exploration and planning using deep skill graphs. In Marina Meila and Tong Zhang, editors, *Proceedings of the 38th International Conference on Machine Learning*, volume 139 of *Proceedings of Machine Learning Research*, pages 521–531. PMLR, 18–24 Jul 2021.
- [4] Chenjia Bai and Rushuai Yang. Constrained ensemble exploration for unsupervised skill discovery, 2024. URL <https://github.com/Baichenjia/CeSD>.
- [5] Chenjia Bai, Rushuai Yang, Qiaosheng Zhang, Kang Xu, Yi Chen, Ting Xiao, and Xuelong Li. Constrained ensemble exploration for unsupervised skill discovery. In *Proceedings of the 41st International Conference on Machine Learning, ICML’24*. JMLR.org, 2024.
- [6] Kate Baumli, David Warde-Farley, Steven Hansen, and Volodymyr Mnih. Relative variational intrinsic control. *Proceedings of the AAAI Conference on Artificial Intelligence*, 35(8):6732–6740, May 2021. doi: 10.1609/aaai.v35i8.16832. URL <https://ojs.aaai.org/index.php/AAAI/article/view/16832>.
- [7] Mohamed Ishmael Belghazi, Aristide Baratin, Sai Rajeswar, Sherjil Ozair, Yoshua Bengio, Aaron Courville, and R Devon Hjelm. Mine: Mutual information neural estimation. In *Proceedings of the 35th International Conference on Machine Learning, ICML’18*. JMLR.org, 2018.
- [8] Yuri Burda, Harrison Edwards, Amos Storkey, and Oleg Klimov. Exploration by random network distillation. In *International Conference on Learning Representations*, 2019.
- [9] Victor Campos. Explore, discover and learn: Unsupervised discovery of state-covering skills, 2020. URL <https://github.com/victorcamos7/edl>.
- [10] Victor Campos, Alexander Trott, Caiming Xiong, Richard Socher, Xavier Giro-I-Nieto, and Jordi Torres. Explore, discover and learn: Unsupervised discovery of state-covering skills. In Hal Daumé III and Aarti Singh, editors, *Proceedings of the 37th International Conference on Machine Learning*, volume 119 of *Proceedings of Machine Learning Research*, pages 1317–1327. PMLR, 13–18 Jul 2020.
- [11] Mathilde Caron, Ishan Misra, Julien Mairal, Priya Goyal, Piotr Bojanowski, and Armand Joulin. Unsupervised learning of visual features by contrasting cluster assignments. In H. Larochelle, M. Ranzato, R. Hadsell, M.F. Balcan, and H. Lin, editors, *Advances in Neural Information Processing Systems*, volume 33, pages 9912–9924. Curran Associates, Inc., 2020.
- [12] Benjamin Eysenbach, Abhishek Gupta, Julian Ibarz, and Sergey Levine. Diversity is all you need: Learning skills without a reward function. In *International Conference on Learning Representations*, 2019.
- [13] Benjamin Eysenbach, Ruslan Salakhutdinov, and Sergey Levine. The information geometry of unsupervised reinforcement learning. In *International Conference on Learning Representations*, 2022. URL <https://openreview.net/forum?id=3wU2UX0voE>.
- [14] Carlos Florensa, Yan Duan, and Pieter Abbeel. Stochastic neural networks for hierarchical reinforcement learning. In *International Conference on Learning Representations*, 2017.
- [15] Karol Gregor, Danilo Jimenez Rezende, and Daan Wierstra. Variational intrinsic control. *ArXiv preprint arXiv:1611.07507*, 2016.
- [16] Abhishek Gupta, Benjamin Eysenbach, Chelsea Finn, and Sergey Levine. Unsupervised meta-learning for reinforcement learning. *ArXiv*, abs/1806.04640, 2018. URL <https://api.semanticscholar.org/CorpusID:48364213>.

- [17] Tuomas Haarnoja, Aurick Zhou, Pieter Abbeel, and Sergey Levine. Soft actor-critic: Off-policy maximum entropy deep reinforcement learning with a stochastic actor. In *International Conference on Machine Learning*, pages 1861–1870. PMLR, 2018.
- [18] Arnav Kumar Jain, Lucas Lehnert, Irina Rish, and Glen Berseth. Maximum state entropy exploration using predecessor and successor representations. In *Thirty-seventh Conference on Neural Information Processing Systems*, 2023. URL <https://openreview.net/forum?id=tFsxtqGmkn>.
- [19] Zheyuan Jiang, Jingyue Gao, and Jianyu Chen. Unsupervised skill discovery via recurrent skill training. In S. Koyejo, S. Mohamed, A. Agarwal, D. Belgrave, K. Cho, and A. Oh, editors, *Advances in Neural Information Processing Systems*, volume 35, pages 39034–39046. Curran Associates, Inc., 2022.
- [20] Minae Kwon, Sang Michael Xie, Kalesha Bullard, and Dorsa Sadigh. Reward design with language models. In *The Eleventh International Conference on Learning Representations*, 2023. URL <https://openreview.net/forum?id=10uNUgI5Kl>.
- [21] Pawel Ladosz, Lilian Weng, Minwoo Kim, and Hyondong Oh. Exploration in deep reinforcement learning: A survey. *Information Fusion*, 85:1–22, 2022. ISSN 1566-2535. doi: <https://doi.org/10.1016/j.inffus.2022.03.003>. URL <https://www.sciencedirect.com/science/article/pii/S1566253522000288>.
- [22] Michael Laskin and Hao Liu. Cic: Contrastive intrinsic control for unsupervised skill discovery, 2022. URL <https://github.com/rll-research/cic>.
- [23] Michael Laskin and Denis Yarats. Urlb: Unsupervised reinforcement learning benchmark, 2025. URL https://github.com/rll-research/url_benchmark.
- [24] Michael Laskin, Hao Liu, Xue Bin Peng, Denis Yarats, Aravind Rajeswaran, and Pieter Abbeel. Unsupervised reinforcement learning with contrastive intrinsic control. In S. Koyejo, S. Mohamed, A. Agarwal, D. Belgrave, K. Cho, and A. Oh, editors, *Advances in Neural Information Processing Systems*, volume 35, pages 34478–34491. Curran Associates, Inc., 2022.
- [25] Misha Laskin, Denis Yarats, Hao Liu, Kimin Lee, Albert Zhan, Kevin Lu, Catherine Cang, Lerrel Pinto, and Pieter Abbeel. URLB: Unsupervised reinforcement learning benchmark. In *Proceedings of the Neural Information Processing Systems Track on Datasets and Benchmarks*, 2021.
- [26] Timothy P Lillicrap, Jonathan J Hunt, Alexander Pritzel, Nicolas Heess, Tom Erez, Yuval Tassa, David Silver, and Daan Wierstra. Continuous control with deep reinforcement learning. *ArXiv preprint arXiv:1509.02971*, 2015.
- [27] Jordan Litman. Curiosity and the pleasures of learning: Wanting and liking new information. *Cognition and Emotion*, 19(6):793–814, 2005. doi: [10.1080/02699930541000101](https://doi.org/10.1080/02699930541000101). URL <https://doi.org/10.1080/02699930541000101>.
- [28] Bo Liu, Xingchao Liu, Xiaojie Jin, Peter Stone, and qiang liu. Conflict-averse gradient descent for multi-task learning. In A. Beygelzimer, Y. Dauphin, P. Liang, and J. Wortman Vaughan, editors, *Advances in Neural Information Processing Systems*, 2021.
- [29] Hao Liu and Pieter Abbeel. Aps: Active pretraining with successor features. In Marina Meila and Tong Zhang, editors, *Proceedings of the 38th International Conference on Machine Learning*, volume 139 of *Proceedings of Machine Learning Research*, pages 6736–6747. PMLR, 18–24 Jul 2021.
- [30] Hao Liu and Pieter Abbeel. Behavior from the void: Unsupervised active pre-training. In M. Ranzato, A. Beygelzimer, Y. Dauphin, P.S. Liang, and J. Wortman Vaughan, editors, *Advances in Neural Information Processing Systems*, volume 34, pages 18459–18473. Curran Associates, Inc., 2021.
- [31] Xin Liu. Comsd: Balancing behavioral quality and diversity in unsupervised skill discovery, 2025. URL <https://github.com/liuxin0824/ComSD>.

- [32] Xin Liu, Yaran Chen, Guixing Chen, Haoran Li, and Dongbin Zhao. Balancing state exploration and skill diversity in unsupervised skill discovery. *IEEE Transactions on Cybernetics*, 2025.
- [33] Aviv Navon, Aviv Shamsian, Idan Achituve, Haggai Maron, Kenji Kawaguchi, Gal Chechik, and Ethan Fetaya. Multi-task learning as a bargaining game. In Kamalika Chaudhuri, Stefanie Jegelka, Le Song, Csaba Szepesvari, Gang Niu, and Sivan Sabato, editors, *Proceedings of the 39th International Conference on Machine Learning*, volume 162 of *Proceedings of Machine Learning Research*, pages 16428–16446. PMLR, 17–23 Jul 2022.
- [34] Alexander Nikulin, Vladislav Kurenkov, Denis Tarasov, and Sergey Kolesnikov. Anti-exploration by random network distillation. In *International Conference on Machine Learning*, pages 26228–26244. PMLR, 2023.
- [35] Aaron van den Oord, Yazhe Li, and Oriol Vinyals. Representation learning with contrastive predictive coding. *arXiv preprint arXiv:1807.03748*, 2018.
- [36] Seohong Park, Jongwook Choi, Jaekyeom Kim, Honglak Lee, and Gunhee Kim. Lipschitz-constrained unsupervised skill discovery. In *International Conference on Learning Representations*, 2022. URL <https://openreview.net/forum?id=BGvt0ghNgA>.
- [37] Seohong Park, Kimin Lee, Youngwoon Lee, and Pieter Abbeel. Controllability-aware unsupervised skill discovery. In Andreas Krause, Emma Brunskill, Kyunghyun Cho, Barbara Engelhardt, Sivan Sabato, and Jonathan Scarlett, editors, *Proceedings of the 40th International Conference on Machine Learning*, volume 202 of *Proceedings of Machine Learning Research*, pages 27225–27245. PMLR, 23–29 Jul 2023.
- [38] Seohong Park, Oleh Rybkin, and Sergey Levine. METRA: Scalable unsupervised RL with metric-aware abstraction. In *The Twelfth International Conference on Learning Representations*, 2024.
- [39] Deepak Pathak, Pulkit Agrawal, Alexei A. Efros, and Trevor Darrell. Curiosity-driven exploration by self-supervised prediction. In Doina Precup and Yee Whye Teh, editors, *Proceedings of the 34th International Conference on Machine Learning*, volume 70 of *Proceedings of Machine Learning Research*, pages 2778–2787. PMLR, 06–11 Aug 2017.
- [40] Deepak Pathak, Dhiraj Gandhi, and Abhinav Gupta. Self-supervised exploration via disagreement. In Kamalika Chaudhuri and Ruslan Salakhutdinov, editors, *Proceedings of the 36th International Conference on Machine Learning*, volume 97 of *Proceedings of Machine Learning Research*, pages 5062–5071. PMLR, 09–15 Jun 2019.
- [41] Roben Delos Reyes, Kyunghwan Son, Jinhwan Jung, Wan Ju Kang, and Yung Yi. Curiosity-driven multi-agent exploration with mixed objectives. *arXiv preprint arXiv:2210.16468*, 2022.
- [42] Andrew G. Barto Richard S. Sutton. *Reinforcement Learning, second edition: An Introduction*. Bradford Books, 2018.
- [43] Evgenia Rusak, Patrik Reizinger, Attila Juhos, Oliver Bringmann, Roland S Zimmermann, and Wieland Brendel. InfoNCE: Identifying the gap between theory and practice. In *High-dimensional Learning Dynamics 2024: The Emergence of Structure and Reasoning*, 2024. URL <https://openreview.net/forum?id=6ufuJl2XyE>.
- [44] Jürgen Schmidhuber. Formal theory of creativity, fun, and intrinsic motivation (1990–2010). *IEEE Transactions on Autonomous Mental Development*, 2(3):230–247, 2010. doi: 10.1109/TAMD.2010.2056368.
- [45] John Schulman, Filip Wolski, Prafulla Dhariwal, Alec Radford, and Oleg Klimov. Proximal policy optimization algorithms. *ArXiv preprint arXiv:1707.06347*, 2017.
- [46] Archit Sharma, Shixiang Gu, Sergey Levine, Vikash Kumar, and Karol Hausman. Dynamics-aware unsupervised discovery of skills. In *International Conference on Learning Representations*, 2020. URL <https://openreview.net/forum?id=HJgLR4KvH>.
- [47] Lucy Xiaoyang Shi, Joseph J. Lim, and Youngwoon Lee. Skill-based model-based reinforcement learning. In *Conference on Robot Learning*, 2022.

- [48] DJ Strouse, Kate Baumli, David Warde-Farley, Volodymyr Mnih, and Steven Stenberg Hansen. Learning more skills through optimistic exploration. In *International Conference on Learning Representations*, 2022. URL <https://openreview.net/forum?id=cU8rknuhxc>.
- [49] Yuval Tassa, Yotam Doron, Alistair Muldal, Tom Erez, Yazhe Li, Diego de Las Casas, David Budden, Abbas Abdolmaleki, Josh Merel, Andrew Lefrancq, et al. Deepmind control suite. *ArXiv preprint arXiv:1801.00690*, 2018.
- [50] Oriol Vinyals, Timo Ewalds, Sergey Bartunov, Petko Georgiev, Alexander Sasha Vezhnevets, Michelle Yeo, Alireza Makhzani, Heinrich Küttler, John P. Agapiou, Julian Schrittwieser, John Quan, Stephen Gaffney, Stig Petersen, Karen Simonyan, Tom Schaul, H. V. Hasselt, David Silver, Timothy P. Lillicrap, Kevin Calderone, Paul Keet, Anthony Brunasso, David Lawrence, Anders Ekermo, Jacob Repp, and Rodney Tsing. Starcraft ii: A new challenge for reinforcement learning. *ArXiv*, abs/1708.04782, 2017.
- [51] Rooshy Yang. Becl: Behavior contrastive learning for unsupervised skill discovery, 2023. URL <https://github.com/Rooshy-yang/BeCL>.
- [52] Rushuai Yang, Chenjia Bai, Hongyi Guo, Siyuan Li, Bin Zhao, Zhen Wang, Peng Liu, and Xuelong Li. Behavior contrastive learning for unsupervised skill discovery. In *Proceedings of the 40th International Conference on Machine Learning*, ICML’23. JMLR.org, 2023.
- [53] Yucheng Yang, Tianyi Zhou, Qiang He, Lei Han, Mykola Pechenizkiy, and Meng Fang. Task adaptation from skills: Information geometry, disentanglement, and new objectives for unsupervised reinforcement learning. In *The Twelfth International Conference on Learning Representations*, 2024.
- [54] Denis Yarats, Rob Fergus, Alessandro Lazaric, and Lerrel Pinto. Reinforcement learning with prototypical representations. In Marina Meila and Tong Zhang, editors, *Proceedings of the 38th International Conference on Machine Learning*, volume 139 of *Proceedings of Machine Learning Research*, pages 11920–11931. PMLR, 18–24 Jul 2021.
- [55] Tianhe Yu, Saurabh Kumar, Abhishek Gupta, Sergey Levine, Karol Hausman, and Chelsea Finn. Gradient surgery for multi-task learning. In *Proceedings of the 34th International Conference on Neural Information Processing Systems*, NIPS ’20, Red Hook, NY, USA, 2020. Curran Associates Inc. ISBN 9781713829546.
- [56] Rui Zhao, Yang Gao, P. Abbeel, Volker Tresp, and W. Xu. Mutual information state intrinsic control. In *International Conference on Learning Representations*, 2021.

A Related Works

A.1 Unsupervised Reinforcement Learning

URL aims to train general-purpose policies capable of rapid adaptation to diverse downstream tasks. This is achieved through the design of intrinsic objectives or rewards that guide exploration without relying on explicit external feedback. URL typically involves two stages: (1) pretraining, where agents develop foundational behaviors driven by intrinsic motivation, and (2) fine-tuning, where these behaviors are adapted to task-specific objectives.

URLB [25] categorizes existing URL algorithms into three primary groups:

1. Data-based approaches encourage agents to explore novel states by maximizing state entropy, fostering diverse experiences during pretraining. Notable methods include APT [30], which utilizes particle-based entropy estimators to maximize the distance between k-nearest neighbors (kNN) in observation embeddings. ProtoRL [54] builds on this idea by incorporating prototypical representation learning, inspired by SWaV [11], to enhance exploration efficiency. CIC [24] extends ProtoRL by introducing skills, positioning CIC as both a data-based and competence-based method.
2. Knowledge-based approaches aim to improve an agent’s understanding of environmental dynamics by maximizing prediction errors, thus incentivizing the exploration of novel or poorly understood states. The Intrinsic Curiosity Module (ICM) [39] encourages exploration by rewarding agents based on the error in predicting future state transitions. Reyes et al. [41] extended this idea by incorporating the prediction of joint observations. On the other hand, disagreement-based methods [40] quantify uncertainty through an ensemble of predictive models, rewarding states where model predictions diverge significantly. Random Network Distillation (RND) [8] measures novelty via the prediction error of a random, fixed target network, where higher errors indicate unfamiliar states. Nikulin et al. [34] enhanced this idea by applying Feature-wise Linear Modulation.
3. Competence-based approaches, often referred to as unsupervised skill discovery, seek to develop a diverse repertoire of skills without relying on external rewards. These methods are grounded in information-theoretic principles, typically maximizing MI between skill embeddings and state, or trajectories to ensure meaningful and diverse behaviors. For instance, VIC [15] maximizes controllability of skills by setting MI between skills and final state, given the initial state as an objective. DIAYN [12] encourages diversity by maximizing MI between skills and states while ensuring skills are distinguishable. BeCL [52] leverages contrastive learning to enhance skill discriminability by maximizing MI between trajectories generated from the same skill; this also has a side effect that maximizes the entropy in the limiting case.

Our approach synthesizes principles from data-based, knowledge-based, and competence-based methods, drawing on models such as CIC [24], RND [8], CeSD [5], and BeCL [52]. Specifically, we address the limitations of these models in balancing exploration and skill diversity by introducing novel methods for integrating them.

A.2 Unsupervised Skill Discovery

Competence-based approaches, commonly referred to as unsupervised skill discovery, have garnered significant attention in recent years due to their potential to enable agents to acquire diverse, discriminative behaviors without external supervision. It focuses on enabling agents to learn distinct, discriminating behaviors without external supervision. Skill diversity has been shown to be critical for downstream task performance, both empirically and theoretically [12, 24, 53]. This is often achieved by maximizing the MI between states or trajectories with skills, encouraging agents to develop diverse and meaningful behaviors. Key contributions in this area include works by [15, 14, 12, 46, 6].

However, these studies [10, 48, 36] have highlighted limitations in traditional MI-based methods, noting that maximizing MI between states and skills can lead to suboptimal exploration. It is also theoretically shown that such approach can not construct an optimal policy for some downstream tasks [13, 53]. There are some methods to address this when the observation space is Cartesian coordinate space [36, 56]; while effective in specific navigation tasks, these approaches impose strong assumptions and are less adaptable to general situation. To address these limitations, alternative approaches introduce auxiliary exploration mechanisms and refined training techniques aimed at enhancing exploration. While many methods focus on modifying the objective functions—such as

DIAYN, BeCL, CeSD, ComSD, and CSD—others explore architectural innovations and dynamic exploration strategies, as seen in DSG [3], EDL [10], and ReST [19]. These techniques aim to promote diverse exploration without relying solely on objective modifications.

B Difference with Former Studies

Prior to our work, two representative methods for jointly considering exploration and diversity are CeSD and ComSD. However, our method departs from these approaches in several important ways, which will be explained in detail. Note that on URLB, our approach achieves 20.91% and 35.01% higher returns than CeSD and ComSD, respectively.

B.1 Difference with CeSD

Instead of diversifying skills using MI, CeSD maximizes exploration using the entropy, while adding a regularization term for diversifying skills. This approach mitigates the paucity of exploration while simultaneously accounting for a diverse array of skills. Unfortunately, the algorithm is time-consuming because it includes clustering states. The paper avoids this bottleneck by choosing a subset of states for clustering, which would lead to inaccurate estimation of clustering and, therefore, instability of training. Also, their regulation on diversity does not work if the state distribution of different skills does not intersect. Such an effect can be seen in the 2D maze experiment; other methods like BeCL or DIAYN separate skills effectively, while CeSD does not. This may be advantageous in low dimension environment like a 2D maze because one can fully cover the whole space. However, in high-dimensional domains such as URLB, insufficient separation of skills degrades downstream task performance, as established by our Theorem 1.

B.2 Difference with ComSD

Similar to ComSD, our approach aims to balance the diversity and exploration objectives. ComSD uses the entropy of trajectory $H(\tau)$ as a exploration objective, and negative entropy of trajectory conditioned to skill $-H(\tau|z)$ as a diversity objective. $H(\tau)$ is estimated using a particle-based approach and $H(\tau|z)$ is estimated using a variational approach. To balance exploration and diversity, ComSD employs a specialized weighting mechanism called Skill-based Multi-objective Weighting (SMW), which assigns different optimization objectives to different skills; some skills emphasizing diversity while others prioritize exploration. However, this selective assignment does not necessarily lead to optimal overall performance. ComSD’s method merely differentiates each skill’s repulsiveness from others, which does not guarantee an ideal trade-off between exploration and diversity. Moreover, it lacks a solid theoretical foundation to justify the weighting strategy.

In contrast, our method explicitly aims to maximize both exploration and diversity, grounded in the concept of gradient conflict, which has been extensively studied in prior research [55, 28, 33]. By directly addressing the conflicts between exploration and diversity gradients, our method achieves a more stable and theoretically justified optimization process.

C Objectives and Rewards

z denote a skill, $\phi(s)$ denote a encoded state, and NN_k denote a k nearest neighbor.

Neglected the loss for training state encoders.

r^{part} is a particle-based entropy estimation, and r^{contr} is a contrastive-based MI estimation; the specific reward varies slightly depending on the method. The canonical MI objective by InfoNCE is defined as:

$$r^{part} = \sum_{i=1}^n \log \|z_i - \text{NN}_k(z_i)\|, \quad r^{contr} = \mathbb{E} \left[\frac{\exp(f(s_t^{(1)}) \cdot f(s_t^{(2)})/\kappa)}{\sum_{s_j \in S^{-1} \cup \{s_t^{(2)}\}} \exp(f(s_t^{(1)}) \cdot f(s_j)/\kappa)} \right] \quad (6)$$

Table 3: Comparison of Algorithms. Intrinsic Objectives and Rewards of each methods are shown.

Algorithm	Intrinsic Objective	Intrinsic Reward (r_t^i)
APT	$H(\phi(s))$	r^{part}
ICM	$\mathbb{E}_\tau[\sum_t \gamma^t r_t^i]$	$\frac{\eta}{2} \ \hat{\phi}(s_{t+1}) - \phi(s_{t+1})\ _2^2$
RND	$\mathbb{E}_\tau[\sum_t \gamma^t r_t^i]$	$\ f(x_t) - f(x_t)\ ^2$
CIC	$H(\tau) - H(\tau z)$	$r^{part} + \log q(\tau z)$
DIAYN	$H(z) - H(z s) + H(a s, z)$	$\log q(z s) - \log p(z)$
DADS	$H(s' s) - H(s' s, z)$	$\log q(s' s, z) - \log \sum_{i=1}^K q(s' s, z_i)$
BeCL	$I(s^{(1)}; s^{(2)})$	r^{contr}
CeSD	$H(s) + \alpha \cdot \sum_{s \in \mathcal{S}} d^{\pi_i}(s) - d^{\hat{\pi}_i}(s) $	$r^{part} + \alpha / (S_i^{pe} \setminus S_i^{clu} + \lambda)$
ComSD	$H(\tau) - H(\tau z)$	$r^{part} + \alpha \cdot r^{contr}$
AMPED (Ours)	$\alpha \cdot H(s) + \beta \cdot \mathcal{L}_{RND} + I(s^{(1)}; s^{(2)})$	$\alpha \cdot r^{part} + \beta \cdot \ \hat{f}(x_t) - f(x_t)\ ^2 + r^{AnInfo}$

D Proof of the theorem

Assume a finite state space \mathcal{S} with cardinality S , and a finite horizon H . Suppose we are given skill-conditioned policies $\pi(a | s, z)$ with a finite number of skills and a downstream task. Let π^* be the optimal policy and $\rho^* \in \Delta(\mathcal{S}^H)$ be a corresponding state distribution. Also set z_* as a best policy in the sense that $z_* = \operatorname{argmin}_z d(\rho^*, \rho_z)$. We denoted the total variation of two probability distributions by $d(\rho_1, \rho_2) = \frac{1}{2} \|\rho_1 - \rho_2\|_1$.

Theorem 1. Define $\delta = \min_{i \neq j} d(\rho_{z_i}, \rho_{z_j})$, $\varepsilon = d(\rho^*, \rho_{z_*})$. Assume that skills are diversified enough, so that $\Delta \equiv \delta - 2\varepsilon > 0$.

Draw n i.i.d. roll-outs $S^{(1)}, \dots, S^{(n)} \sim \rho^*$ and form the empirical distribution $\hat{\rho}$. Consider the greedy skill selector $\hat{z} := \operatorname{argmin}_z d(\hat{\rho}, \rho_z)$. Then

$$\Pr[\hat{z} \neq z_*] \leq 2^{S^H} \exp\left(-\frac{n\Delta^2}{2}\right) \quad (7)$$

In terms of confidence level $\eta \in (0, 1)$, if

$$n \geq \frac{2}{\Delta^2} (S^H \log 2 - \log \eta) \quad (8)$$

we have $\Pr[\hat{z} \neq z_*] \leq \eta$.

Proof.

Step 1. A sufficient condition for correct selection.

Define $\hat{d} := d(\hat{\rho}, \rho^*)$. Triangular inequality gives $d(\hat{\rho}, \rho_{z_*}) \leq d(\rho^*, \rho_{z_*}) + d(\hat{\rho}, \rho^*) = \varepsilon + \hat{d}$. If

$$\hat{d} < \frac{\Delta}{2} = \frac{\delta}{2} - \varepsilon, \text{ i.e. } \delta > 2(\varepsilon + \hat{d}),$$

then $\hat{z} = z_*$ because for every $z \neq z_*$, by triangular inequality,

$$d(\hat{\rho}, \rho_z) \geq d(\rho_{z_*}, \rho_z) - d(\hat{\rho}, \rho_{z_*}) \geq \delta - (\varepsilon + \hat{d}) > \varepsilon + \hat{d} \geq d(\hat{\rho}, \rho_{z_*}).$$

Hence

$$\Pr[\hat{z} \neq z_*] \leq \Pr[\hat{d} \geq \frac{\Delta}{2}]. \quad (9)$$

Step 2. Convergence of $\hat{\rho}$ to ρ^* .

By Bretagnolle–Huber–Carol (BHC) inequality, for a discrete random variable $X = (X_1, X_2, \dots, X_k)$

$$\Pr\left[\sum_{i=1}^k |X_i - np_i| \geq 2\lambda\sqrt{n}\right] \leq 2^k e^{-2\lambda^2}, \quad X \sim \text{Mult}(n, \mathbf{p}).$$

Since $\hat{\rho} = \frac{1}{n} \sum_{i=1}^n \mathbf{1}_{S^{(i)}}$, one can consider empirical distribution as $\frac{X}{n}$ with $k = S^H$; if we let X_i as a number of occurrence of τ_i in $\{S^{(i)}\}_{i \leq n}$, where τ_i is an i th trajectory in $\mathcal{S}^H = \{\tau_1, \tau_2, \dots, \tau_{S^H}\}$. So

$$\hat{d} = \frac{1}{2} \|\hat{\rho} - \rho^*\|_1 = \frac{1}{2n} \sum_{\tau \in \mathcal{S}^H} |\hat{\rho}(\tau) - \rho^*(\tau)|$$

Substituting $\lambda = \varepsilon\sqrt{n}$ into the BHC inequality gives

$$\Pr[\hat{d} \geq \varepsilon] \leq 2^k \exp(-2n\varepsilon^2)$$

Now taking $\varepsilon = \frac{\Delta}{2}$ and combining with (9) gives

$$\Pr[\hat{z} \neq z_*] \leq 2^{S^H} \exp\left(-\frac{n\Delta^2}{2}\right)$$

In terms of confidence level $\eta \in (0, 1)$,

$$n \geq \frac{2}{\Delta^2} (S^H \log 2 - \log \eta) \Rightarrow \Pr[\hat{z} \neq z_*] \leq \eta$$

□

E Toy Experiment on AnInfoNCE

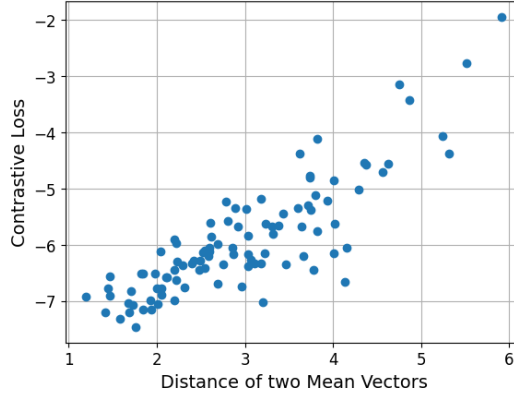


Figure 9: Effect of mean vector’s distance on Loss. Toy example showing that the AnInfoNCE objective has a positive correlation with distance between two distributions. Loss was calculated by sampling 1000 points from two 5-dimensional Gaussian distributions.

A toy experiment was conducted to evaluate the behavior of the AnInfoNCE objective as a function of inter-distribution separation. Two mean vectors were first drawn independently from the standard normal distribution and used to parameterize two Gaussian distributions with identity covariance. AnInfoNCE was then estimated by Monte Carlo sampling from each distribution. Empirically, we observe that the AnInfoNCE loss increases monotonically with the Euclidean distance between the two mean vectors, indicating that larger separations yield higher objective values; see Figure 9. This monotonic relationship highlights the ability of AnInfoNCE to promote diversity between learned skill, in contrast to the CeSD objective, which collapses to zero whenever the support sets of the two distributions do not overlap.

F Implementation Details

F.1 Maze Environments

The maze environments are adapted from the open-source EDL implementation by [9]. In this setup, the observation is given as $\mathcal{S} \in \mathbb{R}^2$, which represents the current position, while the action is given as

$\mathcal{A} \in \mathbb{R}^2$, corresponding to the velocity and direction. The agent observes only its current position and does not have access to the locations of walls, which must be inferred through interaction with the environment. At the start of each episode, the agent’s initial state is uniformly sampled within a 1×1 tile. Table 4 summarizes the details and topological characteristics of each maze used in the experiments.

Table 4: Environment detail of square-maze used for evaluation.

Parameter	Value
State space	$\mathcal{S} \in \mathbb{R}^2$
Action space	$\mathcal{A} \in [-0.95, 0.95]^2$
Episode length	50
Size: Square maze (Figure 12)	5×5
Size: Tree maze (Figure 5 and Figure 11)	7×7

F.2 Network Architectures for Maze Experiments

All code was based on the open-source EDL implementation by [9]. We used PPO [45] as our on-policy algorithm, with both policy and value functions parameterized by three hidden layers of size 128 and ReLU activations. The policy network takes the concatenated state and goal vectors, passes them through three 128-unit MLP layers, then applies a tanh output scaled by the action range. The critic shares the same three-layer backbone but outputs a single scalar Q-value given (s, a) .

For intrinsic rewards, we employed three specialized networks: a CIC encoder comprising a state network that maps the state vector through two 128-unit hidden layers to an n -dimensional embedding and a predictor network that takes the concatenated pair of these embeddings (size $2n$), processes it through two 128-unit hidden layers, and outputs an n -dimensional prediction; an RND network comprising predictor and frozen target MLPs (each with two 128-unit hidden layers) mapping observations to a n -dimensional feature space, where the mean squared prediction error defines r_{rnd} ; and a BeCL encoder implemented as a three-layer 128-unit MLP that maps observations to an n -dimensional skill embedding for the AnInfoNCE loss, encouraging non-overlapping skill distributions.

F.3 URLB Environments

The Walker domain focuses on training a biped constrained to a 2D vertical plane to acquire balancing and locomotion skills [25]. It includes four downstream tasks: *Stand*, *Walk*, *Flip*, and *Run*. The observation space is defined as $\mathcal{S} \in \mathbb{R}^{24}$, and the action space as $\mathcal{A} \in \mathbb{R}^6$.

The Quadruped domain involves training a four-legged agent for balance and locomotion within a 3D environment. This domain includes four tasks (Figure 10): *Stand*, *Walk*, *run*, and *flip*. The observation space is $\mathcal{S} \in \mathbb{R}^{78}$, and the action space is $\mathcal{A} \in \mathbb{R}^{16}$.

The Jaco domain is designed for manipulation tasks using a 6-DoF robotic arm equipped with a three-finger gripper. It includes four tasks: *Reach Top Left*, *Reach Top Right*, *Reach Bottom Left*, and *Reach Bottom Right*. The observation space is $\mathcal{S} \in \mathbb{R}^{55}$, and the action space is $\mathcal{A} \in \mathbb{R}^9$.

F.4 Network Architectures for URLB Experiments

This section describes the network architecture of our method. At the beginning of each episode, a skill vector z is sampled, where the default setting uses a one-hot encoding with `skill_dim` = 16. This skill vector is concatenated with the processed observation features and used as input to the policy, value, and intrinsic reward modules.

The raw observation is first processed by a four-layer convolutional encoder, where each layer has 32 channels and uses Rectified Linear Unit (ReLU) activations. The encoder’s output feature map is then flattened into a latent feature vector of dimensions (`repr_dim` = $32 \times 35 \times 35$). The resulting feature vector is combined with the skill vector before being forwarded to the downstream networks.

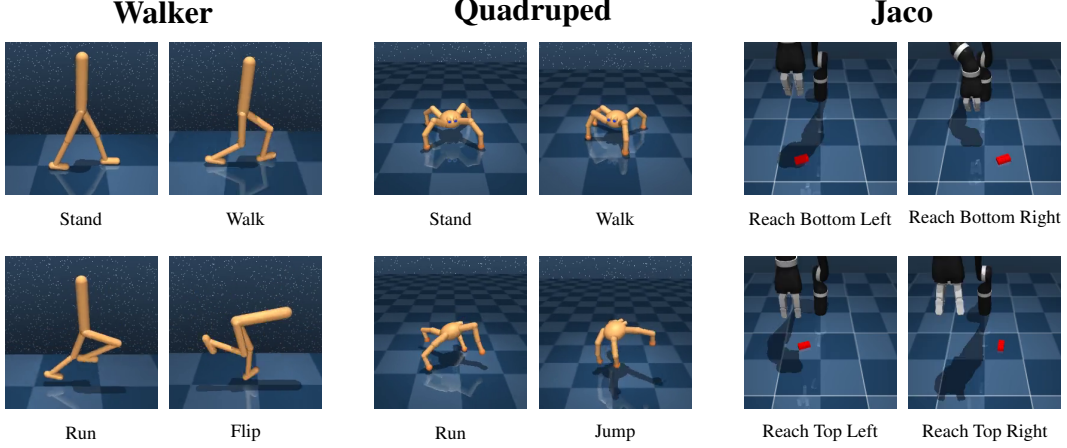


Figure 10: Visualization of the downstream tasks used in the Walker, Quadruped, and Jaco domains.

For decision making, the actor network processes this combined observation and skill vector through a trunk consisting of a linear layer, layer normalization, and hyperbolic tangent (Tanh) activations. The resulting feature is passed through two fully connected layers with 1024 hidden dimensions and ReLU activations, and finally projected to the action space to produce the action distribution. The critic network applies the same trunk structure to the combined representation. It then concatenates the resulting features with the action, and processes them through two additional hidden layers with 1024 dimensions each to estimate the Q-values.

The RND module constructs a predictor-target architecture by copying the observation encoder. Both the predictor and the frozen target network share the same initial encoder and are extended with a multilayer perceptron (MLP) composed of two hidden layers of 1024 dimensions, producing representations of dimensions $\text{rnd_rep_dim} = 1024$. The predictor is trained to minimize the mean-squared error relative to the target’s output.

The CIC module integrates three coordinated components, which consist of a state encoder that transforms both the current and next observation features into embeddings within the skill space, a skill projection network that embeds the sampled skill vector, and a predictor network that takes the concatenated state and next-state embeddings and transforms them into a representation aligned with the skill embedding. All components use MLP with hidden layers of 1024 dimensions, and the module is optimized using a contrastive predictive coding (CPC) objective to encourage alignment between state transitions and the correct skill representation. The state encoder’s outputs are used to calculate the r_{entropy} , based on kNN distances.

The BeCL module takes observation features (excluding the skill vector) and processes them through an embedding network with two hidden layers of 1024 dimensions to produce a compact representation. This representation is then passed through a projection head, which includes another hidden layer with 1024 dimensions and an output layer, producing outputs that match the skill dimension. This layered architecture enables the module to generate embeddings that are optimized for contrastive learning, effectively encouraging skill discrimination in the learned space.

During fine-tuning, we employ a Soft Actor-Critic (SAC)–based skill selector to adaptively choose a skill vector given the current observation. SAC offers off-policy sample efficiency and entropy-regularized stability, which help balance exploration and exploitation. The skill selector consists of a policy network and a value network. The policy network maps observations to a discrete distribution over skills. It consists of a linear layer followed by layer normalization and a Tanh activation, then two fully connected layers with 256 hidden dimensions and ReLU activations, producing logits over the skill space. A skill is sampled from this distribution using an epsilon-greedy strategy. The critic network uses the same input processing as the policy network. It then maps the resulting feature through two fully connected layers with 256 hidden dimensions to produce Q-values for each skill. During training, the critic is updated using temporal difference learning, while the actor is optimized via entropy-regularized policy gradients [17].

In the ϵ -greedy skill selection strategy, the exploration probability ϵ decays exponentially over time, starting from $\epsilon = 1.0$ and gradually decreasing to $\epsilon = 0.01$ with a decay factor of 20000

steps. This encourages early-stage exploration of diverse skills and gradually shifts toward selecting high-performing skills.

F.5 Hyperparameters

Table 6 and Table 5 contains the hyperparameters we use. Hyperparameter values for the Maze environment were adopted directly from the EDL repository [9], while those for the URLB environment follow the defaults provided by the URLB codebase [23]. We perform hyperparameter tuning in URLB, focusing on three key components, intrinsic reward weights (α , β), the projection probability p . We explored values in the ranges $\alpha \in [10^{-3}, 0.1]$, $\beta \in [10^{-3}, 10]$, $p \in [0.5, 1.0]$.

Table 5: Hyperparameter settings for URLB experiments.

Intrinsic reward hyperparameter	Walker	Quadruped	Jaco
skill dimension	16	16	16
contrastive update rate	3	3	3
temperature	0.5	0.5	0.5
alpha (α)	0.01	0.002	0.03
beta (β)	10	8	0.005
projection probability (p)	0.6	0.65	0.8
Number of nearest neighbors (k)	16	16	16
Skill selector hyperparameter	Value		
epsilon start	1.0		
epsilon end	0.01		
epsilon step	20000		
learning rate	3×10^{-4}		
DDPG hyperparameter	Value		
replay buffer capacity	10^6		
warmup frames	4000		
n -step returns	3		
mini-batch size	1024		
discount (γ)	0.99		
learning rate	10^{-4}		
agent update frequency	2		
critic target EMA rate (τ_Q)	0.01		
exploration stddev clip	0.3		
exploration stddev value	0.2		
number of pre-training frames	2×10^6		
number of fine-tuning frames	1×10^5		

Table 6: Hyperparameter settings for Tree Maze experiments.

HyperParameter	Value
learning rate (τ)	3e-4
discount (γ)	0.99
GAE lambda	0.98
entropy lambda	0.025
hidden dim	128
temperature	0.5
alpha (α)	0.01
beta (β)	1e-4
projection probability	0.5
knn k	16
knn clip	5e-4
epoch	50

F.6 URLB Training Pipeline

Algorithm 1 Gradient Surgery

```

1: Given:  $\nabla \mathcal{L}_{\text{diversity}}$ ,  $\nabla \mathcal{L}_{\text{exploration}}$ , probability  $p$ , parameter of critic  $\theta_{\text{critic}}$ , and a learning rate  $\eta$ .
2: if  $\sum(\nabla \mathcal{L}_{\text{diversity}} \cdot \nabla \mathcal{L}_{\text{exploration}}) < 0$  then
3:   With probability  $p$ :
4:      $\nabla \mathcal{L}_{\text{diversity}} \leftarrow \text{Proj}_{\nabla \mathcal{L}_{\text{exploration}}^\perp}(\nabla \mathcal{L}_{\text{diversity}})$ 
5:   Otherwise:
6:      $\nabla \mathcal{L}_{\text{exploration}} \leftarrow \text{Proj}_{\nabla \mathcal{L}_{\text{diversity}}^\perp}(\nabla \mathcal{L}_{\text{exploration}})$ 
7: end if
8:  $\Delta \theta_{\text{critic}} = \eta(\nabla \mathcal{L}_{\text{diversity}} + \nabla \mathcal{L}_{\text{exploration}})$ 
9:  $\theta_{\text{critic}} \leftarrow \theta_{\text{critic}} - \Delta \theta_{\text{critic}}$ 

```

Algorithm 2 Unsupervised Pretraining with Intrinsic Rewards and Gradient Surgery

```

1: Given: number of skills  $n$ , pretraining frames  $N_{\text{PT}}$ , seed frames  $T$ , batch size  $N$ , update interval  $N_{\text{update}}$ , policy  $\pi_\theta$ , critic  $Q_\psi$ 
2: Initialize: replay buffer  $\mathcal{B} \leftarrow \emptyset$ , timestep  $t \leftarrow 0$ 
3: while  $t < N_{\text{PT}}$  do
4:   if  $t \bmod N_{\text{update}} = 0$  then
5:     Sample skill  $z_t \sim \text{Uniform}[1, n]$ 
6:   end if
7:   Collect transition  $(s_t, a_t, s_{t+1}) \sim \pi_\theta(\cdot \mid s_t, z_t)$ ,  $p(s_{t+1} \mid s_t, a_t)$ 
8:   store  $(s_t, a_t, s_{t+1}, z_t)$  in  $\mathcal{B}$ 
9:   if  $t \geq T$  then ▷ begin intrinsic-reward pretraining
10:    Sample batch  $\{(s, a, s', z)\}_{i=1}^N \sim \mathcal{B}$ 
11:    Update encoders:
12:      Minimize contrastive loss (Eq. 4), RND prediction loss, and AnInfoNCE loss (Eq. 5)
13:    Compute intrinsic rewards:
14:      Calculate  $r_{\text{exploration}}$ ,  $r_{\text{diversity}}$  as defined in Sec. 3
15:    Update critic & actor:
16:      Compute gradients for diversity and exploration losses
17:      Apply Gradient Surgery (Alg. 1)
18:      Update policy  $\pi_\theta$  and critic  $Q_\psi$ 
19:    end if
20:     $t \leftarrow t + 1$ 
21: end while

```

Algorithm 3 Fine-Tuning with Extrinsic Rewards and Joint Skill Selector Training

```

1: Given: number of finetuning frames  $N_{\text{FT}}$ , batch size  $N$ , update interval  $U$ , critic  $Q_\psi$ , pretrained policy  $\pi_\theta$ , skill selector  $p_\phi(z \mid s)$ 
2: Initialize: replay buffer  $\mathcal{D} \leftarrow \emptyset$ , timestep  $t \leftarrow 0$ 
3: while  $t < N_{\text{FT}}$  do
4:   Observe state  $s_t$ 
5:   Select skill  $z_t \sim p_\phi(z \mid s_t)$ 
6:   Select action  $a_t \sim \pi_\theta(a \mid s_t, z_t)$ 
7:   Execute  $a_t$  to obtain  $(s_{t+1}, r_t)$ 
8:   Store  $(s_t, a_t, r_t, s_{t+1}, z_t)$  in  $\mathcal{D}$ 
9:   if  $t \bmod U = 0$  then ▷ Update both selector and agent
10:    Sample batch  $\{(s, a, r, s', z)\}_{i=1}^N \sim \mathcal{D}$ 
11:    Update  $\theta, \psi$  using extrinsic reward  $r$ 
12:   end if
13:    $t \leftarrow t + 1$ 
14: end while

```

F.7 Training Time Comparison

Table 7 compares the wall-clock training time of AMPED against a range of baselines on the Walker, Quadrupe, and Jaco domains. Notably, AMPED incurs only a modest increase in runtime relative to competitive methods like CeSD and BeCL despite exceeding their downstream performance (see Figure 6). Although AMPED requires more computation than CIC (an overhead of 3–6 hours), this extra cost yields substantial performance gains over CIC’s purely entropy-based exploration. Overall, these findings demonstrate that AMPED strikes a favorable balance between computational cost and empirical performance.

Table 8 reports fine-tuning times. Because AMPED (Ours) includes the SAC-based skill selector, its fine-tuning incurs a modest overhead of approximately 0.06–0.11 h (4–7 min) compared to baselines such as CIC and BeCL. In future work, we aim to further optimize runtime efficiency—perhaps via more streamlined encoder updates or low-precision training—while preserving the joint handling of exploration and diversity.

Table 7: Pretraining time (hours with decimal minutes) comparison across different algorithms on Walker, Quadrupe, and Jaco domains. Results are computed over 10 random seeds and reported as mean \pm standard deviation.

Domain	AMPED (Ours)	CeSD	CIC	BeCL	APT	RND	DIAYN	DDPG	ComSD
Walker	13.47 \pm 0.06	22.28 \pm 0.08	7.34 \pm 0.18	18.13 \pm 4.65	11.02 \pm 0	5.19 \pm 0.14	7.34 \pm 0.14	4.34 \pm 0.03	7.5 \pm 0.03
Quadrupe	13.62 \pm 0.1	23.01 \pm 0.0	7.6 \pm 0.21	13.42 \pm 2.72	11.18 \pm 0.01	5.45 \pm 0.02	6.96 \pm 1.37	4.49 \pm 0.05	7.74 \pm 0.03
Jaco	13.72 \pm 0.03	22.76 \pm 0.07	7.61 \pm 0.03	14.88 \pm 3.11	11.39 \pm 0.03	6.4 \pm 1.09	8.11 \pm 0.02	4.78 \pm 0.1	7.91 \pm 0.02

Table 8: Fine-tuning time (hours with decimal minutes) comparison across different algorithms on Walker, Quadrupe, and Jaco domains. Results are computed over 10 random seeds and reported as mean \pm standard deviation.

Domain	AMPED (Ours)	CeSD	CIC	BeCL	APT	RND	DIAYN	ComSD
Walker	0.35 \pm 0	0.7 \pm 0	0.26 \pm 0	0.24 \pm 0	0.23 \pm 0	0.36 \pm 0	0.37 \pm 0.01	0.25 \pm 0
Quadrupe	0.35 \pm 0.01	0.73 \pm 0.01	0.29 \pm 0.01	0.29 \pm 0.01	0.26 \pm 0.01	0.44 \pm 0.01	0.4 \pm 0.01	0.28 \pm 0.01
Jaco	0.32 \pm 0.03	0.72 \pm 0.02	0.27 \pm 0.01	0.29 \pm 0	0.26 \pm 0.02	0.28 \pm 0.06	0.38 \pm 0	0.26 \pm 0

F.8 Reproducing Baselines

All baseline methods were integrated from their respective open-source implementations and evaluated under our unified settings. In the Maze environment, DIAYN, CIC, and BeCL were reproduced using the EDL repository [9], and ComSD was imported from its official codebase [31]). Since no public implementation of CeSD exists for the Maze tasks, we followed the visualizations described in the original CeSD paper.

For the URLB, we leveraged the official URLB code [23] to reproduce DIAYN, RND, and APT. CIC, BeCL, and CeSD were run using their respective public implementations [22, 51, 4]. As ComSD lacks an official URLB release, we reimplemented it from its 2D-Maze variant, strictly adhering to the hyperparameters reported in its original publication. Although we employed the unmodified CeSD hyperparameter settings from its codebase and paper, our empirical performance fell short of the authors’ published results.

F.9 Experimental Setup and Reproducibility

All experiments were conducted on a Windows 11 workstation equipped with an AMD Ryzen 7 7700 8-core processor (3.80 GHz), 64GB DDR5 RAM, and an NVIDIA RTX 3060 GPU (12GB GDDR6). Each experiment was run on a single GPU. The detailed wall-clock time for training and fine-tuning are summarized in Table 7 and Table 8.

We implemented all experiments in Python 3.8.10, using PyTorch (v1.9.0+cu111) as the primary deep learning framework. The DeepMind Control suite [49] (dm-control v1.0.8) was used for environment simulation, and agent-environment communication was handled through the dm_env interface (v1.6).

G Additional Experiments in Maze

G.1 Effect of the Number of Skills

Figure 11 illustrates how different methods partition the Tree Maze as the number of skills increases from 5 to 25. Unlike DIAYN and BeCL, which tend to leave large regions unexplored or produce overlapping trajectories, our method fills the entire maze while maintaining clear separation between skills. When using 10 or 15 skills, both CIC and ComSD exhibit substantial mixing between skill regions, whereas AMPED preserves distinct, non-overlapping coverage for each skill. At higher skill counts (20 and 25), all methods begin to overlap simply due to capacity limits, making AMPED’s advantage over ComSD less visually pronounced; nonetheless, it still outperforms CIC in maintaining cleaner skill boundaries. These results confirm that AMPED effectively balances exploration and diversity even as the dimensionality of the skill space grows.

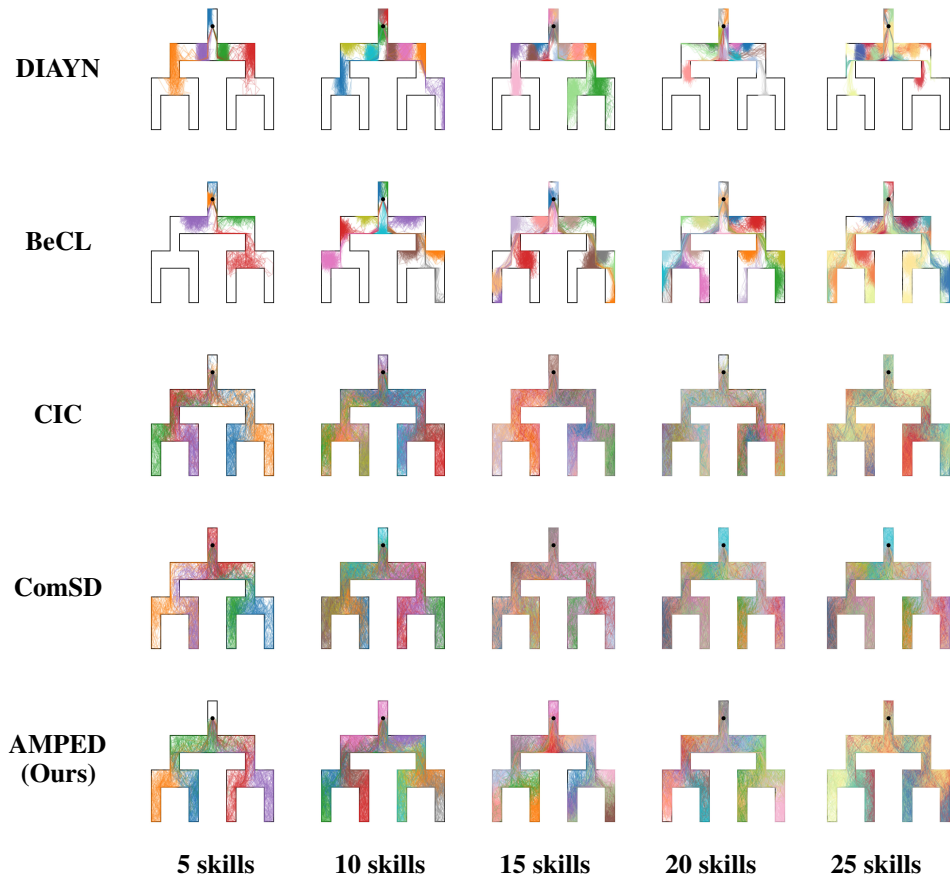


Figure 11: Skill region partitioning in the Tree Maze. This visualization shows the skill allocations of each method as the number of skills increases from 5 to 25. AMPED consistently fills the maze with well-separated regions, whereas DIAYN and BeCL leave gaps, and CIC and ComSD exhibit increasing overlap as the skill count grows.

G.2 Result in Square Maze

In the Square Maze (As shown in Figure 12), AMPED again achieves full coverage and largely distinct skill regions, with only minor overlaps. By contrast, DIAYN and BeCL leave large areas

under-explored or learn only a few broad behaviors, sacrificing either coverage or separation. CIC covers most of the state-space but generates highly entangled trajectories, indicating poor skill disentanglement. ComSD attains coverage similar to AMPED but exhibits more pronounced region mixing. Overall, these results confirm that AMPED not only generalize beyond the Tree Maze but both maximizes exploration and enforces strong skill diversity in the Square Maze as well.

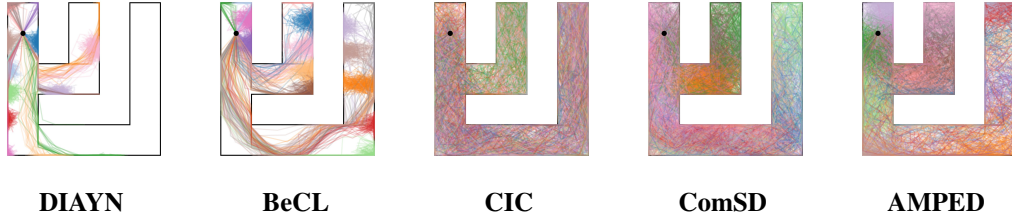


Figure 12: Skill-trajectory coverage in the Square Maze with 15 skills. Each method’s trajectories are shown: AMPED explores every corridor with separated regions, whereas DIAYN and BeCL leave gaps and CIC and ComSD exhibit overlapping trajectories.

G.3 MI and Entropy Estimation

In multi-objective settings, optimizing several objectives can degrade performance on each compared to single-objective training. To evaluate this, we compared the entropy and MI losses against their respective mono-objective baselines, using particle-based entropy estimation and MINE-based MI estimation as in BeCL [7]. Figure 13 confirms that neither objective suffers a significant loss.

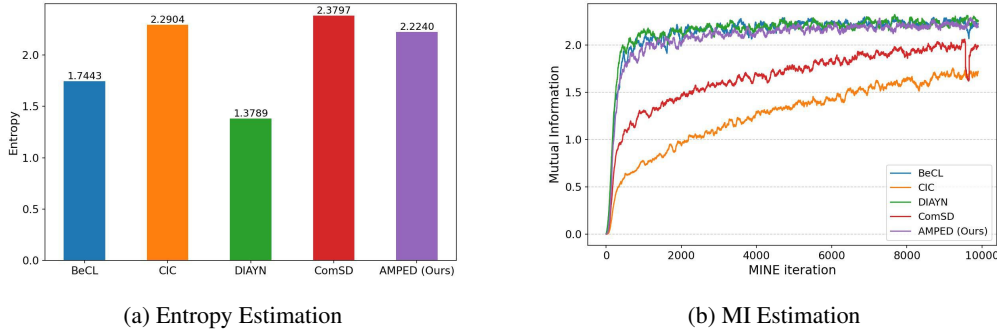


Figure 13: Entropy and MI estimates after pretraining with 10 skills in the Square Maze. (a) Particle-based entropy estimates [30] show that AMPED achieves significantly higher state entropy (exploration) than diversity-focused methods (BeCL, DIAYN), while matching CIC and ComSD. (b) MI estimated via MINE [7] indicates that AMPED attains diversity comparable to BeCL and DIAYN and substantially exceeds CIC and ComSD. Together, these results demonstrate that AMPED simultaneously maximizes exploration and diversity better than existing baselines.

G.4 Evolution of Skills Across Time Steps

As illustrated in Figure 14, early in training (epoch 1), the policy aggressively explores new branches, rapidly expanding its state coverage. By epoch 3 and 5, the trajectory has spanned nearly the entire maze, maximizing exploration. In later stages (epoch 7 and 9), the skill’s path is refined: it begins to adjust which corridors it traverses to carve out distinct regions and increase diversity. Although such clear visualizations are not possible in high-dimensional spaces, this simple sequence provides intuition for how our method first drives broad exploration and then sculpts well-separated skill behaviors.

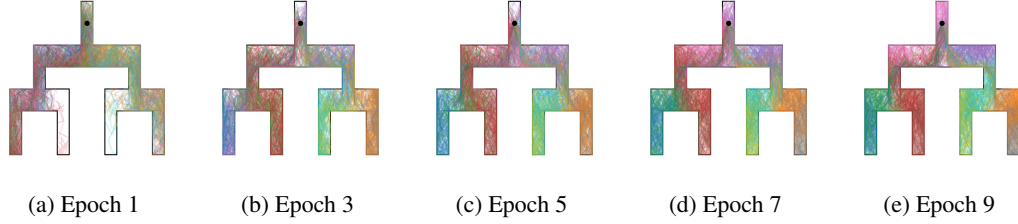


Figure 14: Skill trajectory evolution in the Tree Maze over training epochs. A representative skill’s path is shown at 2-epoch intervals (epochs 1, 3, 5, 7, and 9), illustrating initial rapid expansion of coverage followed by progressive refinement into distinct, well-separated skill regions.

H Numerical Results

H.1 Per-Task Episode Returns on URLB Domains

We report per-task episode returns (mean \pm standard deviation over 10 seeds) following the evaluation protocol of Agarwal et al. [1]. All methods are pretrained for 2M steps with only intrinsic rewards, then finetuned for 100k steps on each downstream task by adding the extrinsic reward. Table 9 presents results on the Walker, Quadruped, and Jaco domains.

AMPED achieves at least second best performance in almost every discipline, and has the highest total sum, which confirms that our method consistently performs well on different tasks. More concretely, AMPED achieves a cumulative total sum of 6415, which is the highest among all methods. The next best is APT with 6362, trailing AMPED by 53 points, and CIC comes third at 5822, well behind by 593 points. These per-task breakdowns confirm that AMPED’s joint handling of entropy, RND, and diversity objectives delivers consistently strong performance across a diverse set of URLB challenges. Although CeSD and ComSD also aim to balance diversity and exploration, AMPED outperforms both on all but one task (Re., top left), demonstrating that our unified objective formulation is more effective.

Table 9: Performance comparison across different algorithms on various tasks. AMPED (ours) is compared with eight baselines across tasks in Walker, Quadruped, Jaco domains. Results are computed over 10 random seeds and reported as mean \pm standard deviation. AMPED is trained without a skill selector for fair comparison.

Domain	Task	AMPED (Ours)	CeSD	CIC	BeCL	APT	RND	DIAYN	DDPG	ComSD
Walker	Flip	686 \pm 133	623 \pm 90	637 \pm 108	625 \pm 66	729 \pm 129	483 \pm 71	329 \pm 39	531 \pm 46	488 \pm 57
	Run	517 \pm 49	377 \pm 89	454 \pm 82	435 \pm 73	542 \pm 73	371 \pm 86	183 \pm 35	327 \pm 115	341 \pm 100
	Stand	947 \pm 19	915 \pm 68	939 \pm 33	953 \pm 11	949 \pm 20	892 \pm 47	716 \pm 127	905 \pm 56	937 \pm 17
	Walk	886 \pm 63	805 \pm 133	874 \pm 67	818 \pm 189	892 \pm 62	792 \pm 139	434 \pm 94	736 \pm 149	826 \pm 111
	sum	3036	2720	2904	2831	3112	2538	1662	2499	2592
Quadruped	Jump	699 \pm 68	529 \pm 160	580 \pm 120	668 \pm 44	720 \pm 32	643 \pm 50	555 \pm 159	337 \pm 129	607 \pm 101
	Run	493 \pm 54	390 \pm 212	442 \pm 72	394 \pm 98	468 \pm 97	435 \pm 34	398 \pm 88	251 \pm 112	336 \pm 91
	Stand	816 \pm 150	853 \pm 40	693 \pm 193	640 \pm 215	821 \pm 192	839 \pm 45	644 \pm 179	511 \pm 253	684 \pm 201
	Walk	816 \pm 116	562 \pm 322	630 \pm 183	635 \pm 205	758 \pm 192	571 \pm 90	404 \pm 200	209 \pm 60	396 \pm 182
	sum	2824	2334	2345	2337	2767	2488	2001	1308	2023
Jaco	Re. bottom left	139 \pm 34	136 \pm 25	135 \pm 19	148 \pm 26	120 \pm 24	101 \pm 24	20 \pm 21	133 \pm 57	126 \pm 24
	Re. bottom right	140 \pm 21	134 \pm 7	152 \pm 23	140 \pm 22	126 \pm 25	115 \pm 24	22 \pm 20	115 \pm 62	111 \pm 41
	Re. top left	130 \pm 38	175 \pm 8	137 \pm 21	123 \pm 35	124 \pm 22	97 \pm 30	22 \pm 22	101 \pm 60	126 \pm 25
	Re. top right	146 \pm 49	97 \pm 29	149 \pm 19	116 \pm 31	113 \pm 25	122 \pm 30	12 \pm 12	87 \pm 53	121 \pm 15
	sum	555	542	573	527	483	435	76	436	484
Total	sum	6415	5596	5822	5705	6362	5461	3747	4243	5099

H.2 Ablation Study on Projection Ratio p

As detailed in Section 4.4, AMPED’s balanced projection ratio mitigates gradient conflicts and enhances skill learning across diverse environments; numerical results are presented in Table 10.

Table 10: Performance comparison under different projection ratio p settings. AMPED (ours) result are computed as return (mean \pm standard deviation) over 10 random seeds, while fixed projection baselines ($p = 0.0$, $p = 1.0$) use 3 seeds each. Our adaptive projection strategy yields the highest return for nearly every tested environment, compared to fixed projection target.

Domain	Task	AMPED (Ours)	$p = 0.0$	$p = 1.0$
Walker	Flip	674 \pm 105	<u>628</u> \pm 55	606 \pm 37
	Run	<u>467</u> \pm 103	427 \pm 44	533 \pm 71
	Stand	951 \pm 38	<u>949</u> \pm 3	931 \pm 12
	Walk	<u>929</u> \pm 19	939 \pm 13	828 \pm 73
	Sum	3021	<u>2943</u>	2898
Quadruped	Jump	720 \pm 34	<u>706</u> \pm 19	661 \pm 34
	Run	<u>494</u> \pm 56	483 \pm 6	501 \pm 29
	Stand	906 \pm 71	859 \pm 109	<u>905</u> \pm 4
	Walk	890 \pm 62	613 \pm 183	<u>626</u> \pm 129
	Sum	3010	2661	<u>2693</u>
Jaco	Re. bottom left	143 \pm 34	<u>133</u> \pm 44	126 \pm 10
	Re. bottom right	144 \pm 27	108 \pm 53	<u>140</u> \pm 17
	Re. top left	140 \pm 41	84 \pm 37	<u>126</u> \pm 29
	Re. top right	154 \pm 49	103 \pm 32	<u>139</u> \pm 34
	Sum	581	428	<u>531</u>

I Ablation Study on Reward Scaling Factor

Table 11: Performance comparison under different α and β settings, where α and β control the relative weight of entropy-based and RND rewards. AMPED (Ours) result are computed as return (mean \pm standard deviation) over 10 random seeds, while each α or β configuration is evaluated using 3 random seeds. Only the denoted hyperparameter is changed and others remain the same as in Appendix F.5.

Domain	Task	AMPED (Ours)	$\alpha = 0$	$\alpha = 100$	$\beta = 0$	$\beta = 1000$
Walker	Flip	674 \pm 105	<u>609</u> \pm 44	587 \pm 74	524 \pm 38	586 \pm 88
	Run	<u>467</u> \pm 103	505 \pm 10	420 \pm 99	382 \pm 29	505 \pm 39
	Stand	<u>951</u> \pm 38	942 \pm 26	956 \pm 6	948 \pm 9	923 \pm 30
	Walk	929 \pm 19	<u>913</u> \pm 43	908 \pm 21	863 \pm 59	878 \pm 94
	Sum	3021	<u>2969</u>	2871	2717	2892
Quadruped	Jump	720 \pm 34	677 \pm 50	<u>710</u> \pm 59	623 \pm 100	648 \pm 61
	Run	<u>494</u> \pm 56	493 \pm 23	459 \pm 122	371 \pm 127	613 \pm 92
	Stand	906 \pm 71	865 \pm 55	837 \pm 117	<u>904</u> \pm 27	875 \pm 23
	Walk	890 \pm 62	844 \pm 58	805 \pm 73	720 \pm 118	<u>852</u> \pm 53
	Sum	3010	2879	2811	2618	<u>2998</u>
Jaco	Re. bottom left	143 \pm 34	94 \pm 31	123 \pm 22	133 \pm 35	<u>134</u> \pm 16
	Re. bottom right	144 \pm 27	111 \pm 15	96 \pm 15	114 \pm 35	<u>118</u> \pm 37
	Re. top left	140 \pm 41	115 \pm 18	159 \pm 24	<u>145</u> \pm 63	121 \pm 3
	Re. top right	154 \pm 49	112 \pm 22	<u>143</u> \pm 18	112 \pm 16	106 \pm 11
	Sum	581	432	<u>521</u>	504	479

In this ablation, we keep every setting in Appendix F.5 fixed except for one of the reward-scaling factors. As shown in Table 11, deviating from the defaults on either α or β degrades the sum of episode returns in most domains. Setting $\alpha = 0$ (no entropy reward) or $\beta = 0$ (no RND reward) leads to substantial drops, while excessively large values ($\alpha = 100$ or $\beta = 1000$) improve some individual tasks but hurt overall performance. The default AMPED weights achieve the best aggregate performance, underscoring the need for balanced scaling between exploration and novelty signals.

J Additional Experiments on Reward Scaling Factor

In Table 12, we present additional ablation results for the entropy reward weight α and the RND reward weight β . In the Walker domain, the average sum return across five (α, β) configurations is 2989.4, which still ranks second among the baselines in Table 9. Notably, the (0.01, 8) setting achieves a sum return of 3323, outperforming all baselines. Similarly, in the Quadrupe domain, the average across the five configurations is 2908.2, exceeding the best baseline performance. Moreover, the (0.002, 10) configuration yields even better performance than our default hyperparameter choice. These results suggest that careful tuning of α and β can yield further improvements for AMPED.

Table 12: Ablation study results under various (α, β) settings. The leftmost column (AMPED) reports the mean \pm std over 10 random seeds; all other columns show single-run returns for each modified hyperparameter configuration.

Domain	Task	AMPED (0.01, 10)	(0.02, 10)	(0.005, 10)	(0.01, 12)	(0.01, 8)
Walker	Flip	674 \pm 105	667	535	599	886
	Run	467 \pm 103	451	354	<u>550</u>	565
	Stand	951 \pm 38	<u>960</u>	942	964	949
	Walk	929 \pm 19	893	891	797	<u>923</u>
	Sum	<u>3021</u>	2971	2722	2910	3323
	Task	AMPED (0.002, 8)	(0.004, 8)	(0.001, 8)	(0.002, 10)	(0.002, 6)
Quadrupe	Jump	720 \pm 34	597	702	710	<u>717</u>
	Run	494 \pm 56	<u>499</u>	276	512	488
	Stand	906 \pm 71	956	792	<u>918</u>	<u>918</u>
	Walk	<u>890</u> \pm 62	833	853	891	869
	Sum	<u>3010</u>	2885	2623	3031	2992

K Additional Experiments on Skill Selection

One of the central motivations for our approach is that the skill selector, responsible for choosing among a diverse, pretrained set of skills, should substantially enhance overall performance. However, an ablation in the Walker domain (3021 with the selector vs. 3036 without it) revealed that adopting the skill selector does not lead to consistent improvements; in fact, performance even degrades in the Walker domain.

To investigate this discrepancy, we designed a complementary experiment isolating each pretrained skill: for each task, we fix a single skill and condition the policy exclusively on that skill during fine-tuning, both for training and evaluation. Specifically, we ran the experiments on the *flip* and *run* tasks in the Walker benchmark, where the selector previously degraded performance, and the *stand* and *walk* tasks in the Quadrupe benchmark—where the selector had been beneficial (3010 with the selector vs. 2824 without it).

The fixed-skill results in Table 13 show that the skill selector underperforms single-skill fine-tuning across three tasks. Crucially, this deficit persists whether the selector had previously appeared beneficial (as in the Quadrupe environments) or not (as in Walker), indicating that the selector itself, rather than domain-specific factors, is the primary bottleneck. Although dedicated fine-tuning benefits from sustained gradient updates targeted at a single skill, the observed performance gap suggests

Table 13: Fine-tuning returns (mean \pm std) over 3 seeds on Walker (flip / run) and Quadruped (stand/walk) tasks under different skill-selection regimes. “Single-Skill” reports the average return across fine-tuning each pretrained skill individually; “Oracle Best Skill” denotes the highest return achieved by the single best skill.

Domain	Task	Skill Selector	Random Skill	Single-Skill	Oracle Best Skill
Walker	Flip	674 \pm 105	686 \pm 133	<u>719</u> \pm 121	913 \pm 3
	Run	467 \pm 103	<u>517</u> \pm 49	503 \pm 74	603 \pm 19
Quadruped	Stand	906 \pm 71	816 \pm 150	<u>911</u> \pm 43	959 \pm 5
	Walk	<u>890</u> \pm 62	816 \pm 116	837 \pm 62	912 \pm 17

that the selector’s learning is hampered, likely by sparse rewards. Consequently, its value estimates remain unstable, leading to suboptimal choices. These findings underscore the need for more robust training strategies for the skill selector.

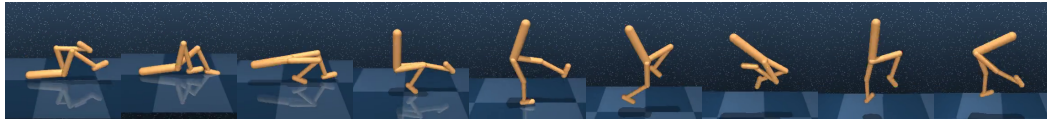
L Visualization of Skills

Figure 15 illustrates the skills acquired during the pretraining stage for each environment.

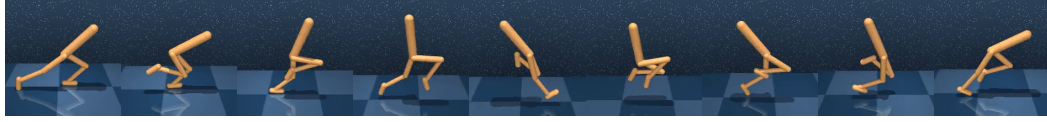
M Limitations

As with any research, our approach presents several limitations that highlight opportunities for future investigation:

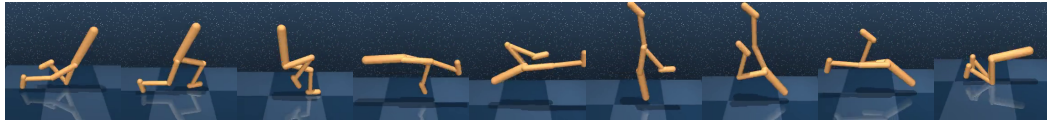
- **Better gradient conflict resolver:** Although PCGrad is easy to implement and powerful, it has few limitations. First, Liu et al. [28] demonstrate that PCGrad does not preserve the original objectives; instead, it merely guarantees convergence to the Pareto set. More advanced gradient conflict-resolution techniques have since been developed; future work can select the method best suited for SBRL.
- **Removing heuristics:** Although we have introduced theory-based gradient surgery to balance exploration and diversity of skills, we still use the rule of thumb such as positive hyperparameters α, β for $r_{\text{total}} = r_{\text{diversity}} + \alpha r_{\text{entropy}} + \beta r_{\text{rnd}}$. Future work should eliminate such empirical rule of thumb.
- **Inaccuracy and inefficiency of Estimators:** AnInfoNCE lacks precision, so future research should consider approaches that tightens the MI bound. And for entropy which has a high computational overhead, one should explore methods that are computationally efficient and capable of functioning effectively in high-dimensional state spaces. Model-based approaches, such as those using normalized flows [2], could be potential solutions.
- **Better objectives:** The diversity term adopted from the BeCL paper influences entropy, leading to gradient conflicts. Future research could focus on developing better objectives that maintain diversity without compromising entropy. In addition to entropy and RND based exploration, there has been a lot of research going on [21]. One may find a better way to explore more efficiently and effectively.
- **Balancing Other Factors Beyond Diversity and Exploration:** While our work primarily focuses on diversity and exploration, other aspects are also being actively studied to improve performance. Exploring how to harmonize our method with these additional aspects could be a valuable direction for future research. For instance, recent studies, such as [37], rewards states that are difficult to reach.
- **Fixed Number of Skills:** The current model treats the number of skills as a fixed hyperparameters, which is of course not ideal across different environments; see Figure G. While too few skills limit overall state coverage, once exploration saturates, adding more skills offers no further benefit. Developing mechanisms to dynamically adjust the number of skills according to the environment’s requirements could enhance flexibility and performance.



Walker: Getting up from the ground



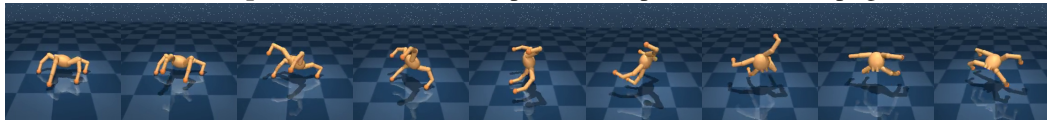
Walker: Stepping forward



Walker: Backward somersault



Quadruped: Recovers from an upside-down position to stand upright



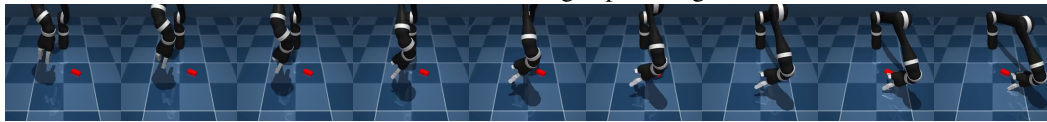
Quadruped: Backward somersault



Quadruped: Clockwise rotational movement



Jaco: Reaches left to grasp the target



Jaco: Reaches toward the right area and grasps the object



Jaco: Upward lifting motion while attempting to grasp the target

Figure 15: Representative skills learned by our method. **Walker** skills include rising from a supine position, stepping forward, and performing a backward somersault. **Quadruped** skills demonstrate self-righting, acrobatic flips, and rotational maneuvers. **Jaco** skills capture precise arm motions such as leftward reaching, rightward grasping, and upward lifting toward a target.